NSE neutrino spectrum

Andrzej Odrzywolek*
M. Smoluchowski Institute of Physics
Jagiellonian University
Reymonta 4
30-059 Krakow
Poland
(Dated: March 13, 2009)

Emission of the neutrinos, including energy spectrum from plasma under Nuclear Statistical Equilibrium is investigated. Particular attention is paid to possible emission of the high energy neutrinos or antineutrinos. To facilitate calculations involving neutrino emission new numerical approach to NSE abundances has been developed. Using appropriate interpolating scheme we are able quickly pick up out of NSE ensemble abundances of species with known neutrino emission. First, we analyze neutrino emission in general conditions using FFN data. Regions in the $T-\rho-Y_e$ space with promising from detectability point of view features are selected. Importance of critical Y_e values with zero net neutronization rate $\dot{Y}_e = 0$ is discussed. Basic spectral features of the NSE neutrino spectrum are presented for a broad range of conditions.

PACS numbers: 97.60.Jd, 26.60.+c, 97.60.-s

I. INTRODUCTION

Neutrino cooling is of paramount importance in the modern astrophysics [1–3]. It governs late stages of stellar evolution, especially massive stars [4, 5], red giant cores [6], white dwarfs [7], core-collapse supernovae [8–13] and evolution of (proto)neutron stars [14]. Other objects where neutrinos play important role are mergers involving neutron star [15, 16], dense accretion disks in e.g. Gamma Ray Bursts (GRB) models [17, 18], type Ia supernovae [19] and X-ray flashes [20].

Usually, neutrinos act as an efficient energy sink, and only the total neutrino emissivity, i.e. amount of energy carried out by the neutrinos is of interest. Additional effect of the net $\nu_e - \bar{\nu}_e$ flux is neutronization of matter crucial for understanding of the nucleosynthesis. Therefore previous research on NSE neutrino emission [21] focused on two functions: (1) $\nu_e - \bar{\nu}_e$ particle emission rates (2) total $\nu_e + \bar{\nu}_e$ energy carried out by the neutrinos. We would like to extend analysis to cover spectral/flavor properties of the NSE neutrino flux.

Much more detailed treatment of the neutrino emission is typical for core-collapse simulations [22, 23] and frequently neglected for other astrophysical objects. However, recently progressively more interest is directed towards spectral properties of the neutrino flux. Neutrino energy is important for core-collapse supernovae, neutrino-induced nucleosynthesis (ν–process, [24–26]), neutrino oscillations and, last but not least, neutrino detection in terrestrial experiments. The latter area is particularly poorly explored. Neutrino spectrum for a bunch of well-recognized neutrino cooling processes rarely is treated in rigorous way. Typical procedure is to use some more or less justified analytical approximate formula for neutrino energy spectrum, with parameters (one or two of them) computed from known neutrino emissivity and average neutrino energy. In this paper we continue effort [27, 28] to calculate spectral properties for important neutrino emission processes, now those involving weak nuclear β transitions.

Neutrino cooling processes can be separated into two classes: (1) thermal processes including e^-e^+ pair annihilation, massive in-medium photon & plasmon decay and neutrino photoproduction (2) weak nuclear processes i.e. $\beta^{\pm}$ decays and $\epsilon^{\pm}$ captures. Noteworthy, for all thermal processes (pair, plasma, photoproduction, bremsstrahlung, neutrino deexcitation of the nuclei) neutronization rate is zero, i.e. change of the proton/neutron ratio is exclusively due to weak nuclear processes. Another important difference is flavor of the produced neutrinos: (1) produces all flavors while (2) only ν_e and $\bar{\nu}_e$. Unfortunately, neutrino oscillations can easily destroy information on thermal and weak components mixing them somewhere between place of emission and distant interaction/detection. Weak nuclear processes often tend to dominate neutrino emission of hot and very dense plasma, at least until matter is still transparent to neutrinos. Particularly, electron captures on both protons and heavy nuclei are progressively more intense with growing density due to Fermi energy $E_F \simeq \mu_e$ crossing capture threshold (Q-value) for increasing number of nuclear species. High

*URL: http://www.ribes.if.uj.edu.pl/; Electronic address: odrzywolek@th.if.uj.edu.pl

temperature additionally enhance emission because many of the nuclei remains in the thermally excited states with larger matrix elements for weak transitions. For temperatures larger than ∼0.5 MeV, significant fraction of equilibrium positrons cause strong $\bar{\nu}_e$ flux due to e^+ captures, particularly on free neutrons.

In contrast to thermal processes, determined entirely (including energy spectrum) by the local thermodynamic properties of matter (e.g. temperature kT and electron chemical potential μ_e), weak nuclear processes depend also on abundances of nuclei. This essentially renders task of calculating neutrino spectrum impossible to achieve, as infinite number of evolutionary tracks leads to unpredictable by simple means output, especially for evolutionary advanced objects[1]. For rapidly evolving object, all we can say, is that neutrino spectrum emitted form plasma is:

$$\phi(\mathcal{E}_\nu) = \sum_k X_k(t)\psi_k(\mathcal{E}_\nu, kT, \mu_e)\ \frac{\rho}{m_p A_k} \tag{1}$$

where ψ_k represent (assumed known, from theory or experiment) spectral shape of single nuclei neutrino emission, and $X_k(t)$ set of usually unknown and rapidly varying abundances. Even today, tracking required number of abundances (few hundred) is impossible in all but simplest one-dimensional models.

Fortunately, if the temperature becomes high enough, nuclei begin to ,,melt" due to photodisintegrations and nuclei re-arrange via strong interactions into thermodynamically the most probable state [29]. This is the Nuclear Statistical Equilibrium (thereafter NSE) approximation [30]. Timescale required to achieve NSE is mainly temperature-dependent [31, 32] and can be approximated as [33]:

$$\tau_{\rm NSE} \sim \rho^{0.2} e^{179.7/T_9 - 40.5} \tag{2}$$

where ρ is density in g/cm^3 and $T_9 = T/10^9$K where T is the temperature. Eq. (2) provide one of the most important constraints limiting use of the NSE approach. While it is typical to assume (2) to be independent of Y_e, actually $Y_e = 0.5$ is assumed in calculation used for $\tau_{\rm NSE}$ estimation [31, 32]. Therefore in plasma with Y_e far from 0.5 caution is required with interpretation of the results, as both under- an over- estimate might be possible. For $kT = 0.2$ MeV, timescale is of the order of the age of the universe, $\tau_{\rm NSE} \sim 10^9$ years, for $kT = 1$ MeV, $\tau_{\rm NSE} \sim 10^{-9}$ seconds. In the core of typical pre-supernova star with $\rho = 10^9$ g/cm^3 and $kT = 0.32$ MeV, $\tau_{\rm NSE} \simeq 2$ days. Typical duration of the Si burning stages depends on stellar mass, from few hours to 3 weeks. During thermonuclear explosion of type Ia supernova in the flame region temperatures grow up to $kT = 0.4 \ldots 0.6$ MeV, and $\tau_{\rm NSE} \simeq 5$ miliseconds, while explosion time is of the order of 1 second.

If additionally both hydrodynamic timescale and weak transmutations rate between protons and neutrons, measured by $\dot{Y}_e$:

$$\dot{Y}_e \equiv \frac{dY_e(t)}{dt} = \lambda_{\nu_e} - \lambda_{\bar{\nu}_e}, \tag{3}$$

where:

$$\lambda_\nu = \sum_k \lambda_\nu^{(k)} \frac{X_k}{A_k}, \quad \lambda_\nu^{(k)} = \int_0^\infty \psi_k(\mathcal{E}_\nu)\ d\mathcal{E}_\nu,$$

are slow[2] compared to $\tau_{\rm NSE}$, we can safely assume quasistatic evolution in the three parameter space usually[3] temperature kT, density ρ and electron fraction Y_e. For given triad (kT, ρ, Y_e) we are able determine abundances of all nuclei. This approximation, called Nuclear Statistical Equilibrium (NSE) is widely used in Fe cores of pre-supernova stars, supernovae, nuclear networks, thermonuclear flames and nucleosynthesis studies. Under NSE conditions neutrino emission is in principle not much different from thermal processes (especially if $\dot{Y}_e = 0$, cf. Sect. IV), and no prior knowledge of abundances is required. This allow e.g. for postprocessing of models with known history of temperature, density and electron fraction. If $Y_e(t)$ is not known we still can use NSE approximation assuming some value, e.g. $Y_e = 0.5$ for symmetric nuclear matter. Unfortunately in the most interesting range of $Y_e = 0.35 \ldots 0.55$ and relatively low temperatures of $kT < 0.5$ MeV, composition (and therefore neutrino emission) is extremely sensitive to small changes in Y_e, cf. Fig. 4, 5. One possible method to overcome this problem is to use so-called tracer particles built-in

---

[1] This situation is however very difficult to describe using statistical methods. Variety of astrophysical objects and processes is closer to complex systems rather than gases.

[2] Slow in the sense of eq. (3), not actual weak rates $\lambda_\nu, \lambda_{\bar{\nu}_e}$, which may be very high.

[3] As noted by [21], relativistically invariant triad $T - n_B - Y_e$ where n_B is conserved baryon number density may be used if General Relativity formulation is required.

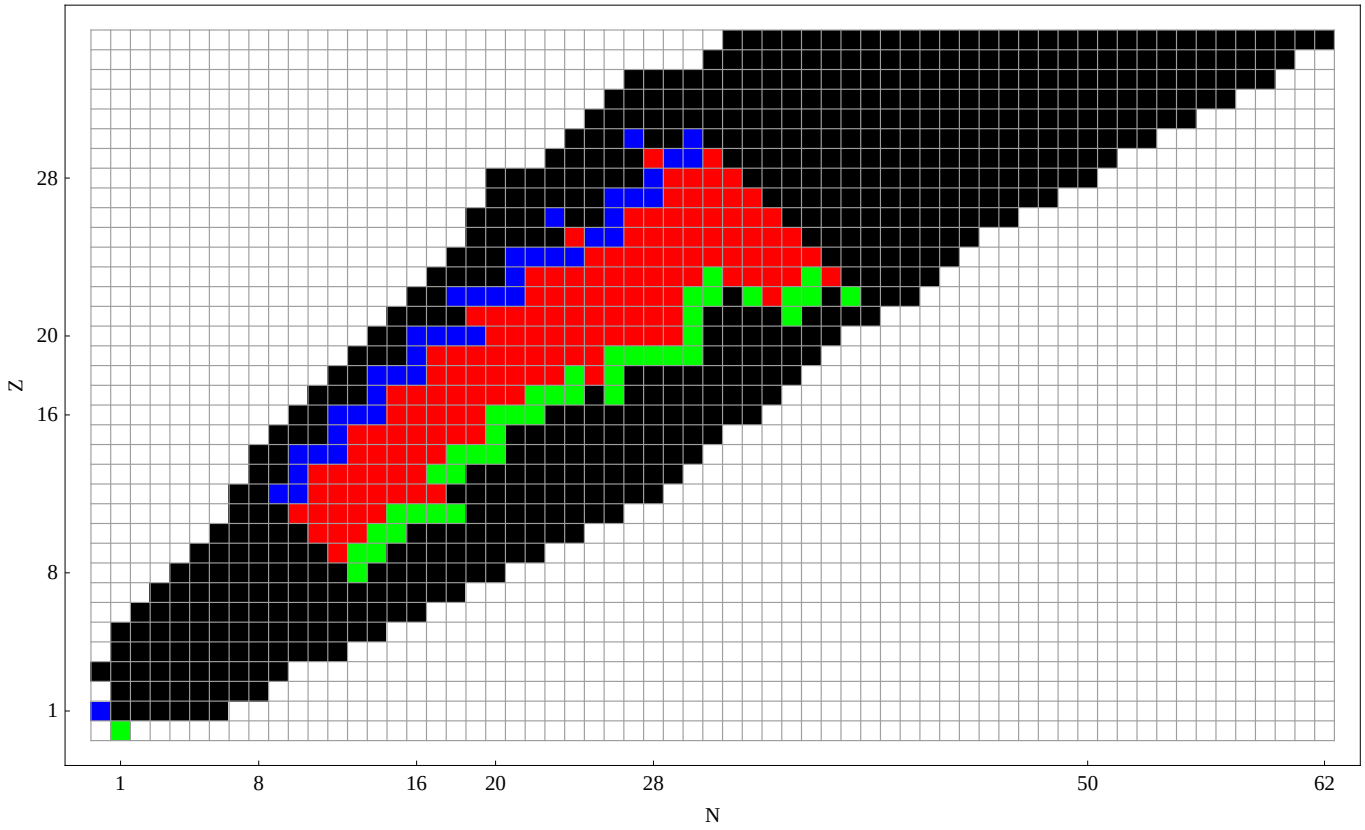

FIG. 1: Nuclides included in the NSE and neutrino emission calculations.

into simulation to remember thermodynamic history of matter and then calculate history of Y_e. Another application of the NSE neutrino emission, described in [21], is subgrid-scale model of nuclear flame energetics in thermonuclear supernovae.

Paper is organized as follows: in Sect. II we present calculations of the Nuclear Statistical Equilibrium and efficient interpolating method to handle abundances, in Sect. III we discuss spectra of individual nuclei under conditions of high temperature and density using solar ^{7}Be neutrinos as an example and finally in Sect. IV we combine results of Sect. II and III to get NSE neutrino emissivities and energy spectra using FFN [34–37] rates. Some concluding remarks and a ,,wish list" for future theoretical neutrino astronomy (calculations of the neutrino spectra) is included in final section.

II. NSE

Well-known equations for the ensemble of $N_{iso}+1$ nuclei in thermal equilibrium [21, 38] are:

$$\sum_{k=0}^{N_{iso}} X_k = 1 \tag{4a}$$

$$\sum_{k=0}^{N_{iso}} \frac{Z_k}{A_k} X_k = Y_e \tag{4b}$$

where abundance X_k for k-th nuclei with atomic number Z_k and mass number A_k is:

$$X_k = \frac{1}{2} G_k(T) \left(\frac{1}{2}\rho N_A \lambda^3\right)^{A_k-1} {A_k}^{5/2} X_n^{A_k-Z_k} X_p^{Z_k} e^{\frac{Q_k}{kT}}. \tag{5}$$

Partition function for k-th nuclei is:

$$G_k(T) = \sum_{i=0}^{i_{max}} (2J_{ik}+1) e^{-\frac{E_{ik}}{kT}} \tag{6}$$

where summation is over all excited states (numbered by the index i) of the k-th nucleus; J_{ik} and E_{ik} are the spin and the excitation energy, respectively. Q_k is the binding energy, ρ, T - density and temperature of the plasma, N_A is the Avogadro number and k - Boltzmann constant. Thermal de'Broglie wavelength used in eq. (5) is:

$$\lambda = \frac{h}{\sqrt{2\pi m_H kT}} \tag{7}$$

where m_H is the mass of the hydrogen atom and h denotes Planck's constant.

NSE equations form high-order polynomial system for unknown proton X_p and neutron X_n abundances. Typical (and actually mere one[4]) method used to solve Eqns. 4 is a standard Newthon-Raphson iteration scheme [21, 39]. Due to complications with numerical precision and unpredictable iteration numbers, rapidly growing with number of species and for low temperatures, procedures are complicated and very hard to parallelize [40]. Moreover, even if we are interested in abundance of single nucleus entire system (4) has to be solved. Such a situation is typical for neutrino spectrum calculations, as usually much more nuclear species are included in NSE than those with known neutrino emission rates. Usually very few of them contribute at non-negligible level, e.g. p, ^{56}Ni and ^{55}Co for ν_e emission at $Y_e = 0.5$. Large part of $kT - \rho - Y_e$ space is completely dominated by processes involving neutrons and protons only. In the course of the research we have faced this problem, as our NSE ensemble included at least 800 nuclides (Fig. 1, black) while FFN tables used include only 189 of them (Fig. 1, red, blue and green). Interpolation of the pre-calculated results has been found to be optimal solution.

To handle results of the NSE calculations efficiently, interpolation seems to be wrong solution. Naively, one might try to interpolate stored proton X_p and neutron X_n abundances obtained from Eq. (4), and get X_k from (5). Unfortunately, this does not work, as even a very small error in X_n or X_p produces enormous errors[5] in X_k due to large (~ 30) integer powers in (5). Another ,,brute force" method is tabulation of every X_k. This might be useful if a few out of NSE species are of interest. This is also the fastest approach. However, for larger number of species amount of stored data becomes very large. Fortunately, we found a compromise, which successfully combines both ideas. Inability to get accurate abundances using interpolated X_n, X_p does not include grid points, as they can be stored with accuracy up to the machine precision or even better if required. First, we calculate abundance of selected species X_k at grid points neighboring given (ρ, T, Y_e) point. Next, we interpolate using computed X_k's. Only proton X_p and neutron X_p abundances need to be tabulated, but several times more (using formula (5) at minimum 8 corners of a cube) computational time is required compared to interpolation of stored X_k values for all nuclei. Additionally, partition function $G_k(T)$, atomic and mass numbers Z_k, A_k and binding energy Q_k has to be stored for all nuclei to use (5). Using (tri)linear interpolation eqns. (4) are fulfilled automatically up to original solving accuracy.

Of course, we still have to solve (4) to generate X_p and X_p tables. Any method e.g. existing codes [39], pre-calculated results or a web service [41] may be used in this purpose. As efficiency and speed of the code is not of primary importance if one use interpolating scheme, Eqns. (4a, 4b) has been solved numerically using MATHEMATICA code[6] for first 800 nuclides available in MATHEMATICA [43] database with temperature dependent partition function. Measured excited states were used only if present in database, otherwise neglected. No Coulomb corrections were applied.

Abundances are then tabulated as a functions of temperature, density and electron fraction and used as input for (tri)linear interpolation. NSE results are checked against available codes/results [21, 39–41] with good agreement.

Determination of NSE abundances is crucial for many applications, including nucleosynthesis, neutrino emission, nuclear energy generation and equation of state. Therefore we have made some tests to verify results and accuracy estimates. Despite known physical issues (temperature-dependent partition function, Coulomb corrections, [21]) one

---

[4] In principle polynomial system might be reduced using Groebner basis methods, especially over rational field. In practice ensemble including protons, neutrons and single heavy nuclei can be solved, but additional components cause Groebner basis algorithms to fail in sense of computational time: no result is returned at all in period of several hours.

[5] This relative error can be estimated as: $\delta(X_n^N X_p^Z) \sim A\, 2^A \delta X$, where δX is typical relative error of X_n (X_p) and A is mass number. For $A \sim 60$ amplification of relative error might be as large as 10^{18} (!) for $X_n \sim X_p \sim 0.5$.

[6] Entire code [42] has approx. 100 lines including database loading, writing C headers, and solving (4) with arbitrary precision. Code is very slow compared to FORTRAN equivalents, a price paid for convenience and simplicity of the programming language of MATHEMATICA. Fortunately, this is not an important issue, as all we want is to generate tables. Later we use interpolators, which are very fast, even compared to FORTRAN codes.

TABLE I: Minimum number of nuclides required to compute *all* abundances above X_{min}.

X_{min}	Z	A	niso	Last included nuclide
10^{-1}	28	56	562	^{56}Ni
10^{-2}	28	57	563	^{57}Ni
10^{-4}	29	59	592	^{59}Cu
10^{-5}	30	60	620	^{60}Zn
10^{-6}	30	61	621	^{61}Zn
10^{-7}	30	63	623	^{63}Zn
10^{-8}	31	63	651	^{63}Ga
10^{-9}	31	65	653	^{65}Ga
10^{-10}	32	66	683	^{66}Ge
10^{-12}	32	68	685	^{68}Ge
10^{-20}	36	75	807	^{75}Kr
10^{-30}	41	87	970	^{87}Nb

of the most important factors is number and selection of species included in equations (4). Even a single one important nuclei missing in NSE ensemble may lead to radically different results[7]. While inclusion of some nuclei seems obvious (p, n , ^{4}He, ^{56}Ni, iron group) further selection is more or less arbitrary. To quantify problem we tried to solve the following: find the maximum required atomic (Z) and mass number (A) to get solution including all species with abundance larger than X_{min}. Results are presented in Table I and Fig. 2. For example, from Table I, if we do not want to miss any of species with abundance above e.g. 10^{-6}, we need at least nuclides up to ^{61}Zn. Nuclei in Fig. 2 are ordered according to [43]; approximate Z and A are included as a tickmarks for a top axis. This estimate gives an upper limit for number of required nuclei. To get true minimal number of nuclides required to get all species above assumed accuracy one have to consider all subsets for entire considered $kT - \rho - Y_e$ space. Number of subsets, given by the Bell number B_n is $B_{800} \simeq 2 \times 10^{1479}$. Therefore, rigorous selection of species is impossible for large sets, and the safest thing to do is to use estimates given by Table I or consider all nuclei available [41].

From Fig. 2 we can conclude that the most primitive NSE including p and n only is not useful, maybe except for very high temperatures, cf. Fig. 3. Inclusion of the alpha particle extends applications to lower temperatures but usually p and n abundances are wrong by few orders of magnitude. To get correct abundances of p and n for lower temperatures entire iron peak has to be included. X_p and X_n are rock-stable if all nuclei below Z=28, A=56 are included. This number might be seriously reduced if we focus on narrow Y_e range and exclude low mass (A=3..16) elements. Anyway, results in Table I indicate, that no more than 1000 nuclei are required to get all abundances above 10^{-30}. While it is possible to solve NSE equation for more than 3000 nuclides [41], it does not change results significantly. Later in the article we use 800 nuclei presented in Fig. 1.

Numerical precision might be another problematic issue. Careful programming with proper handling of round-off errors or arbitrary-precision calculations are required to get correct results.

For completeness we discuss some basic well-known properties of the NSE state. For a very high temperatures above $kT \simeq 0.5$ MeV ($T \simeq 5.8 \times 10^9$ K) no bound nuclei can exist and we have mixture of free neutrons and protons (Fig. 3) plus photons and electrons. As temperature decrease helium is being ,,synthesized" like in Big Bang nucleosynthesis. If temperature drops further more below $kT \simeq 0.35$ MeV ($T \simeq 4 \times 10^9$ K) and NSE is maintained for long enough, heavy most bound nuclei are preferred. Finally, cold catalyzed matter state is a pure (for $Y_e = 0.45$) ^{58}Fe, cf. Fig. 3; for $Y_e = 0.5$ it is ^{56}Ni, of course. This is pretty clear physical picture. Therefore for higher temperatures we expect overwhelming domination of the neutrinos from electron capture on protons and antineutrinos from positron capture on neutrons. These processes will compete with thermal emission, e.g. pair annihilation emissivity grow like $\sim T^9$. For intermediate temperatures, the most abundant helium is extremely resistant for electron capture, but abundance of free nucleons is still important. For lowest temperatures, heavy nuclei dominate, but not every species lead to strong neutrino emission. Note the extremely strong Y_e dependence of the NSE state (Fig. 4). As Y_e dependence for large temperature is trivial (smooth balance between p, n and α abundances) the most interesting is the temperature range where heavy nuclei dominate. Note that, for higher densities, temperature threshold for heavy nuclei formation moves to a little bit higher temperatures. Striking feature of Fig. 4 is a rapid variation of the abundances within range of $Y_e = 0.35 \ldots 0.5$; cf. Fig. 5. NSE clearly prefer k-th nuclei with individual $Y_e^{(k)} \equiv Z_k/A_k$ as close as possible to Y_e

[7] Very illustrative, but unfortunately physically doubtful is case of ^{3}Li i.e. tri-proton. Normally, for $Y_e \gg 0.5$ free protons are abundant. But if ^{3}Li would exist, it should take the role of protons under NSE conditions if density is high enough, cf. Fig. 4.

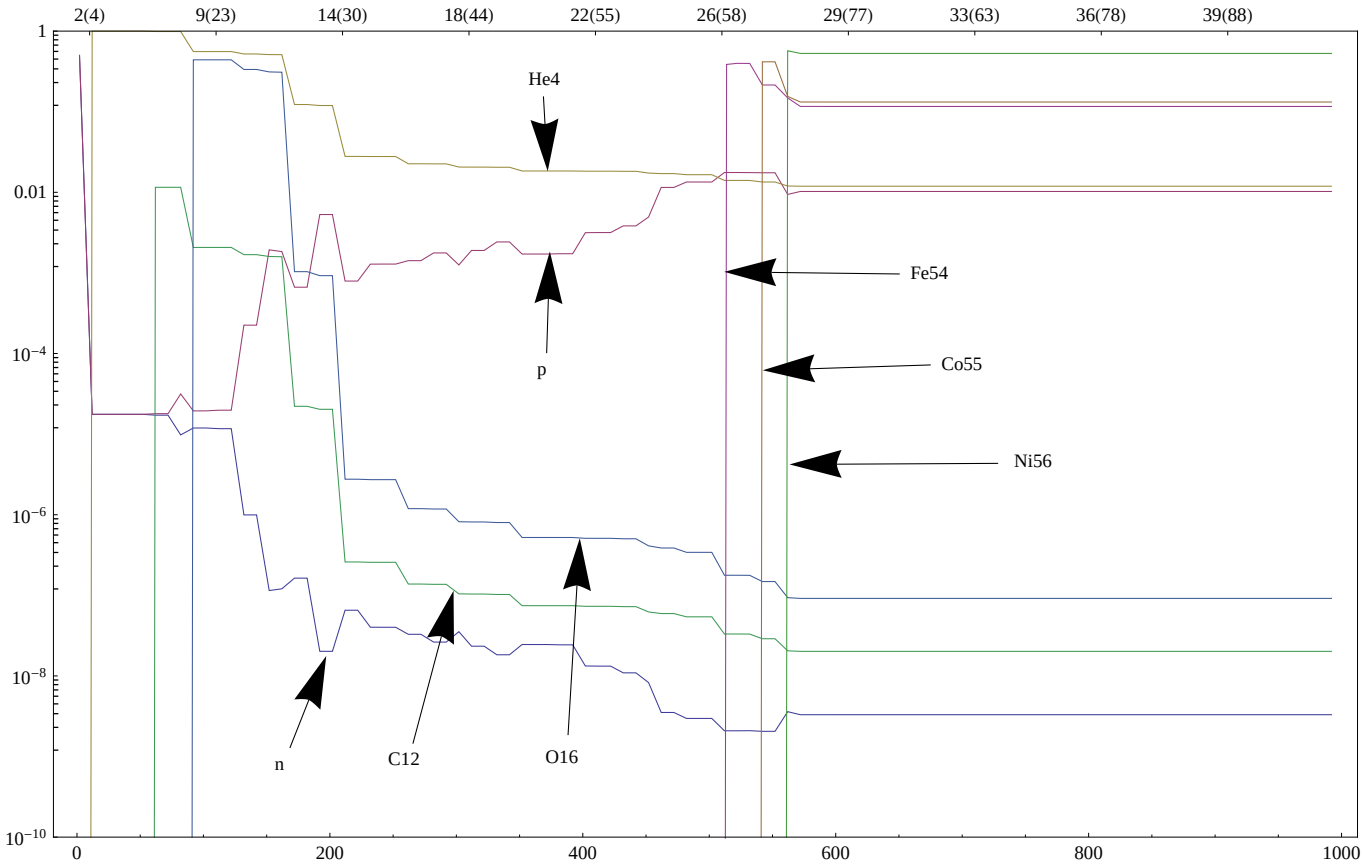

FIG. 2: NSE abundances as a function of the number of the nuclei involved in calculations for $kT = 0.4$ MeV, $\rho = 10^7$ g/cm^3 and $Y_e = 0.5$.

for entire thermodynamic ensemble. For example double magic nuclei ^{78}Ni with largest known neutron excess[8] (lowest $Y_e = 28/78 \simeq 0.36$) dominates for $Y_e < 0.365$ until neutrons (with $Y_e = 0$) take a lead. For opposite side $Y_e > 0.5$ carefull reader will be surprised with large abundance of ^{3}Li i.e. tri-proton. Usually only protons (^{1}H) have $Y_e = 1$. While most of nuclear physicist would deny existence of ^{3}Li at all, we have left this species[9] for illustrative purposes: inclusion of even single nuclei with e.g. unusual Y_e (or other properties) might seriously alter NSE abundances.

We expect strong imprint of rapid abundance variation on neutrino emission. For example, known for large electron capture rate ^{55}Co has non-negligible abundance only in narrow range of $Y_e = 0.47 \ldots 0.5$, cf. Fig. 5.

Note that due to large variations in Fig. 5 even extremely simple analysis is successful. For example, large measured abundance of Fe (iron peak, resulting from ^{56}Ni decay) obviously limit electron capture rate. Nucleosynthesis studies tell us that typical conditions met in astrophysical objects and properties of the nuclei could not lead to enormous ν_e emission, at least if $\bar{\nu}_e$ flux is also small.

III. NEUTRINO SPECTRUM FROM β PROCESSES FOR SINGLE NUCLEUS IN THERMAL BATH

Pioneering theoretical work in this field is due to Bahcall [47, 48] in the context of Solar neutrino spectrum. Further work is therefore limited to numerical upgrades in terms of number of nuclei involved, better nuclear data etc. With notable exception of the Sun [49] and geoneutrinos [50] rigorous treatment of the neutrino spectra from individual nuclei is usually ignored in astroparticle physics. Core-collapse simulations use parameterized approach, cf. e.g.

[8] Neutron excess is equivalent to Y_e: $\eta = 1 - 2Y_e$.

[9] ^{3}Li sometimes is included in nuclide databases with atomic mass 3.030775 and binding energy 2.2676 MeV, but actually such a nuclei should not exist on theoretical ground [44]. Experimental detection [45] has not been confirmed [46]; see also comments in ESNDF data for Li3 at http://ie.lbl.gov/ensdf/.

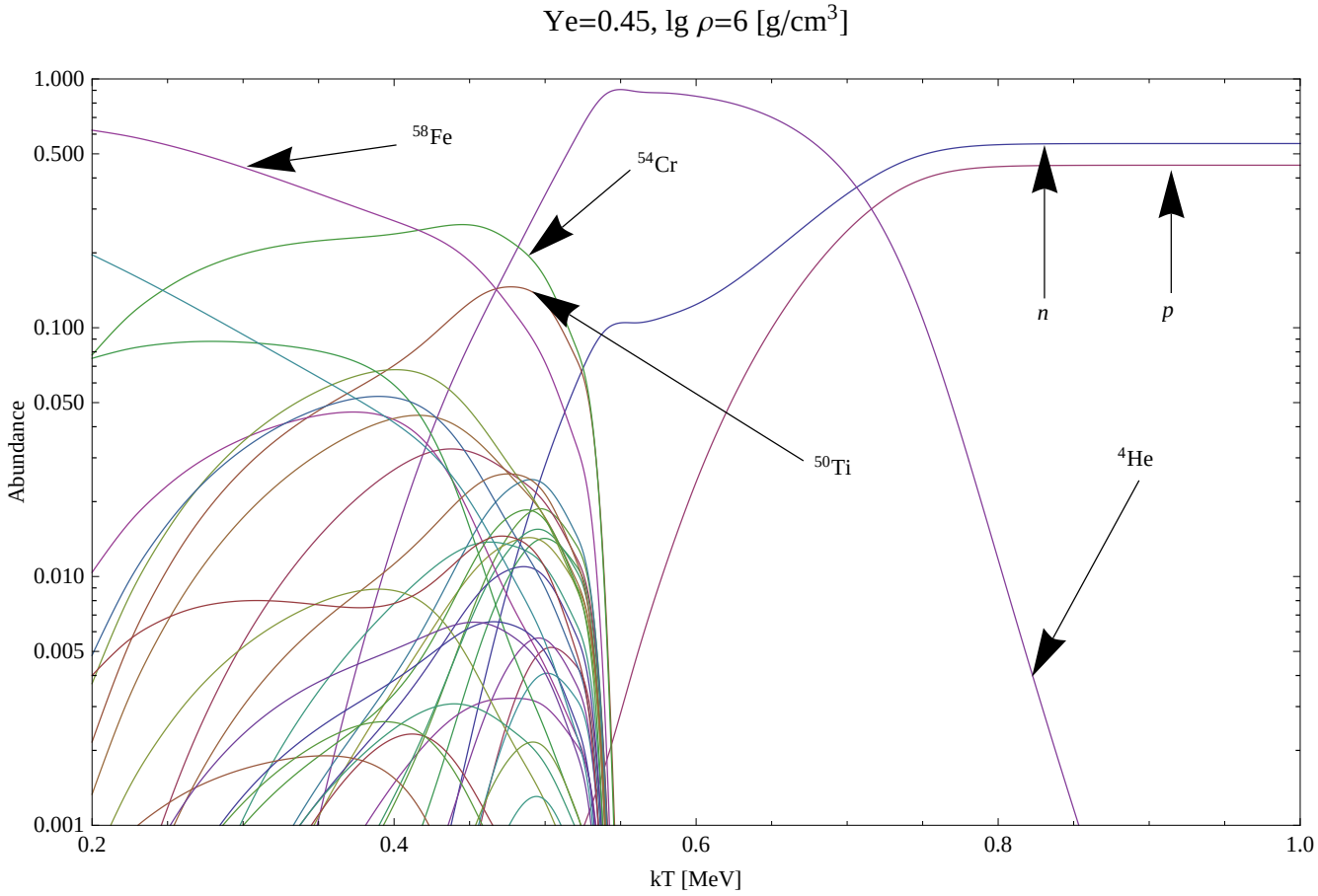

FIG. 3: NSE abundance *versus* temperature.

[22, 51]. Unfortunately, in case of multi-peaked neutrino spectrum this approach simply do not work, cf. Fig. 1 and related comments in [51]. Antineutrino spectrum from all species but neutrons usually is neglected.

Spectrum of neutrinos emitted from single nuclei in astrophysical plasma depends strongly on temperature and chemical potential of the electrons, and positrons as well if $kT \sim m_e = 0.511$ MeV or larger. For example, putting ^{7}Be into solar interior ($kT = 1.35 \times 10^{-3}$ MeV, $\mu_e = 0$) makes little change with respect to terrestrial experiments. It is illustrative to put this nuclei into plasma under conditions typical for evolutionary advanced astrophysical object, e.g. pre-supernova star or supernova.

Let us begin with typical example of continuum electron capture process:

$$^7\mathrm{Be} + e^- \rightarrow ^7\mathrm{Li} + \nu_e$$

In general, assuming inertial target nucleus mass infinite and neglecting various correction factors (screening, Coulomb factor) $\epsilon^{\pm}$ capture rate is proportional to constant matrix element multiplied by physical constants and so-called phase space factor Φ:

$$\Phi_c(\mathcal{E}_\nu, \Delta Q, kT, \mu_e) = \frac{\mathcal{E}_\nu^2(\mathcal{E}_\nu - \Delta Q)\sqrt{(\mathcal{E}_\nu - \Delta Q)^2 - {m_e}^2}}{1 + \exp\left[(\mathcal{E}_\nu - \Delta Q - \mu)/kT\right]}\Theta(\mathcal{E}_\nu - \Delta Q - m_e), \tag{8}$$

where $\mathcal{E}_\nu$ denotes neutrino energy ($\mathcal{E}_{\nu_e}$) for e^- capture and antineutrino energy ($\mathcal{E}_{\bar{\nu}_e}$) for e^+ capture. ΔQ is the energy difference between initial and final state (both can be excited) and m_e is the electron rest mass. Electron chemical potential μ_e includes m_e, and therefore for positrons $\mu_{e^+} = -\mu_{e^-} \equiv -\mu$; kT is the temperature of the electron gas.

It is worth to notice, that by expressing factor (8) by the neutrino (antineutrino) energy rather than electron (positron) energy as usual we have just one formula, as both signs of $\Delta Q + m_e$ are covered, assuming the property $\mathcal{E}_\nu > 0$ obvious.

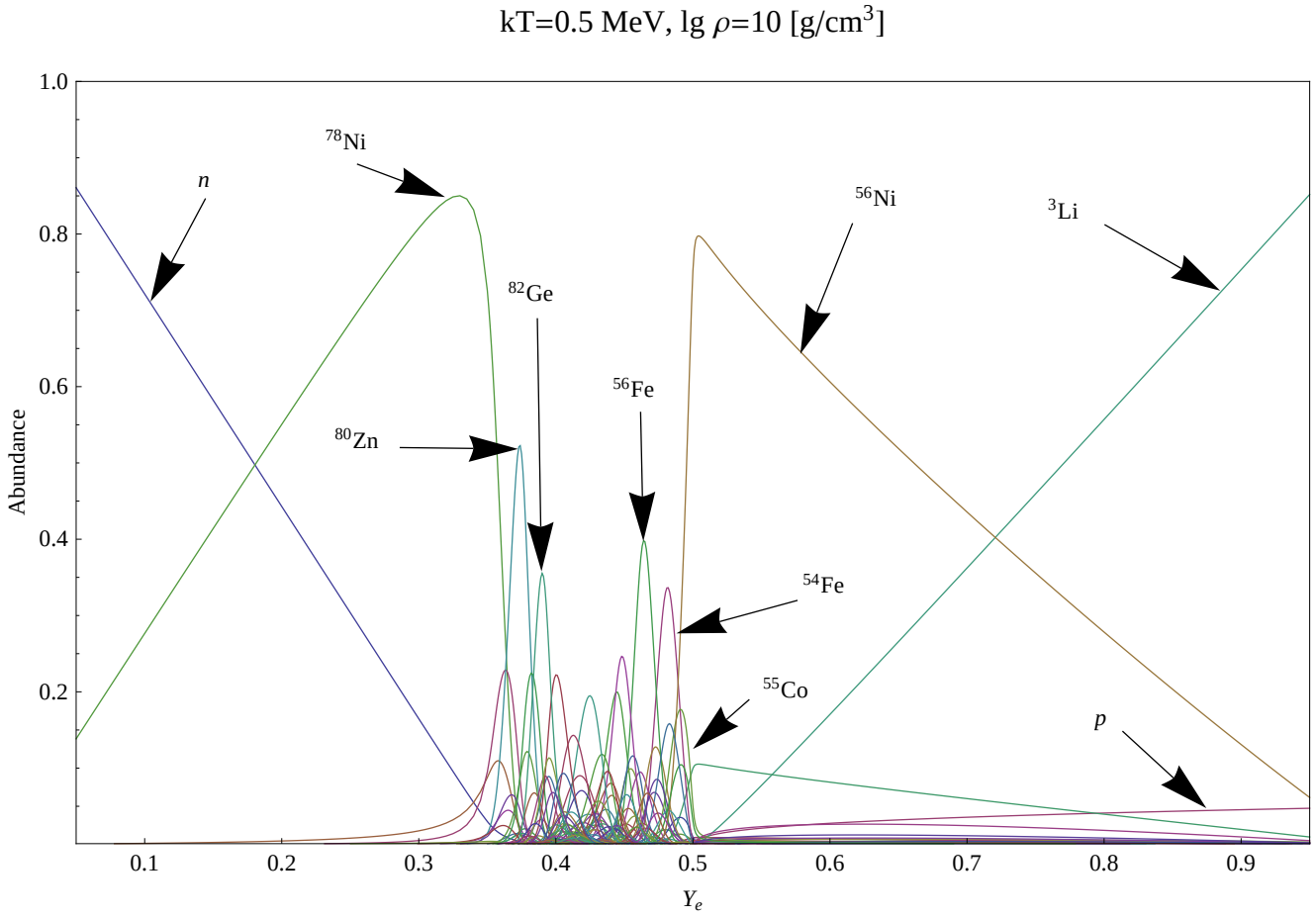

FIG. 4: NSE abundance *versus* electron fraction Y_e.

Neutrino spectrum from $\beta^{\pm}$ decay is proportional to:

$$\Phi_d(\mathcal{E}_\nu, \Delta Q, kT, \mu_e, Z_k) = \frac{\mathcal{E}_\nu^2(\Delta Q - \mathcal{E}_\nu)\sqrt{(\mathcal{E}_\nu - \Delta Q)^2 - {m_e}^2}}{1 + \exp{(\mathcal{E}_\nu - \Delta Q + \mu)/kT}}\Theta(\Delta Q - m_e - \mathcal{E}_\nu) \tag{9}$$

Figure 6 compares neutrino spectrum given by formula (8) with more elaborated result of [52] for solar neutrinos. Results are in good qualitative agreement. In both cases from Fig. 6 neutrino spectrum is simply a line of negligible (Fig. 7, upper-left) in most applications width. The horizontal axis in Fig. 6 is the difference between Q-value (including m_e) and neutrino energy in keV. This is because for solar conditions Q-value for ^{7}Be capture is by many orders of magnitude larger than temperature and chemical potential of the electron gas. If we put ^{7}Be into a plasma where kT or μ is comparable to the Q-value, both capture rate and neutrino spectrum changes dramatically, cf. Fig 7. In general, spectrum shape is a result of the competition between Fermi-Dirac distribution and the unit step function Θ in (8). While e^- kinetic energy always adds to the neutrino energy, for low (solar and lower) temperatures it is negligible compared to $\Delta Q + m_e$. If temperature becomes non-negligible compared to Q-values of nucleus, say $kT > 0.1$ MeV, thermal broadening due to kinetic energy of electrons becomes important and rate enhanced, cf. Fig. 7, upper-right panel. For some of the laboratory stable nuclei electron (positron) capture might be possible for high energy electrons (positrons) from thermal distribution tail.

Increasing density resulting in large μ_e has even a more visible effect, because most of the electrons, not just a small fraction from tail, has large energies. Neutrino spectrum (Fig. 7, lower-left) has a very characteristic shape in this case, with sharp edge on the high $\mathcal{E}_\nu$ end. With increasing μ_e progressively more nuclei becomes unstable to electron capture with continuously growing rate. Lower-right panel in Fig. 6 show combined effect of large kT and μ.

Anyway, possibly the most striking feature of Fig. 7 is not spectrum shape but dramating scale change on the vertical axis. Weak rates are extremely sensitive to both kT and μ mainly due to phase-space factors (8, 9).

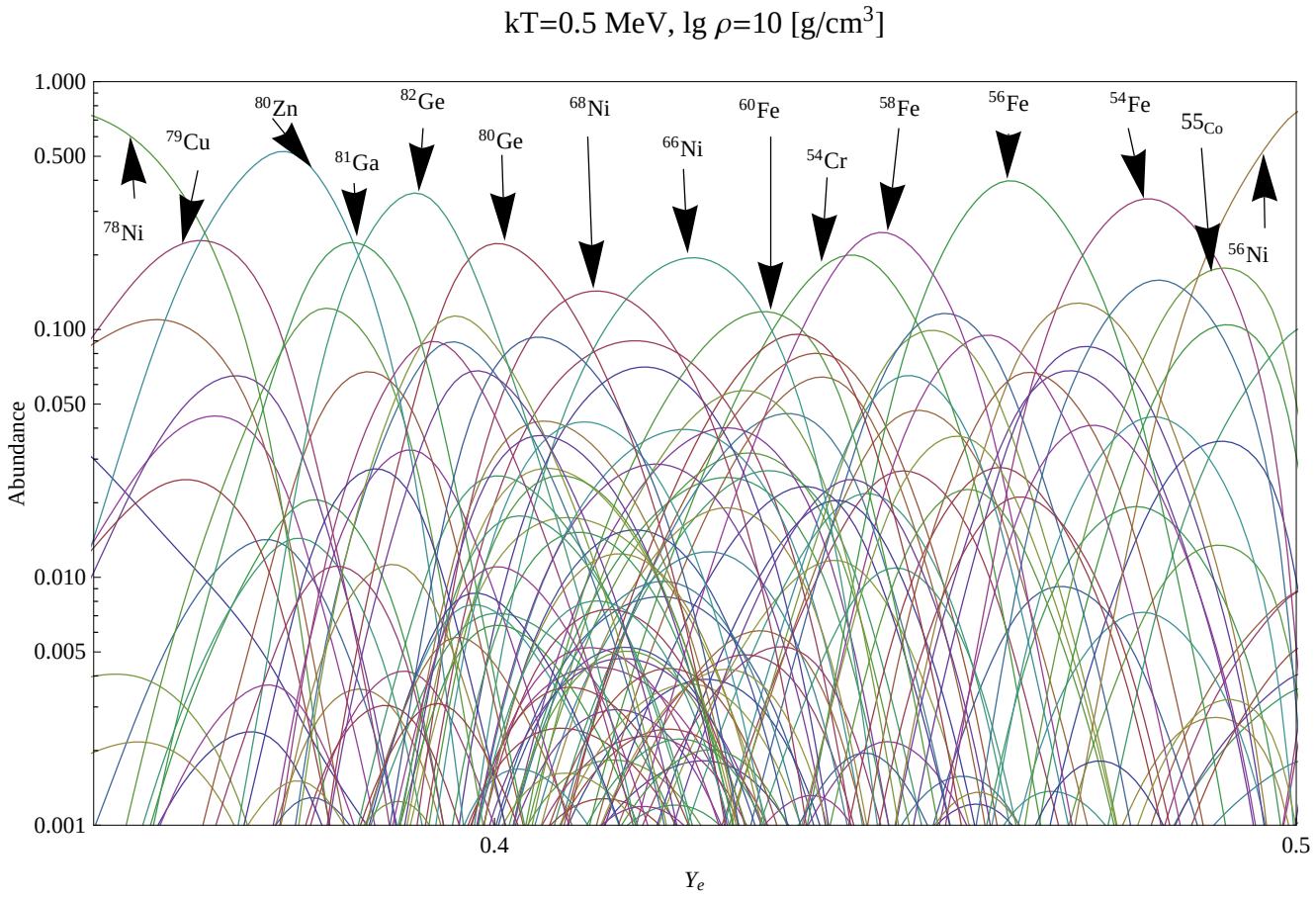

FIG. 5: Zoom of the Fig. 4 into the most interesting range of $Y_e = 0.35 \ldots 0.5$.

IV. NSE NEUTRINO SPECTRA

A. General properties of the NSE neutrino emission

To get neutrino energy spectrum from high temperature astrophysical plasma using NSE approximation for abundances, we need to combine results of Sections II and III. Approach used in our article is nothing particularly new [38], but we provide some general formulae for completeness.

Once abundances X_k has been found from NSE, spectral neutrino emissivity due to e^- (e^+) capture on k-th nuclei is [34–36, 53, 54]:

$$\frac{d\lambda_\nu}{d\mathcal{E}_\nu} = \sum_k X_k \frac{\ln 2}{K} \sum_{i=0}^{i_{max}} \frac{2J_{ik}+1}{G_k(kT)} e^{-\frac{E_{ik}}{kT}} \sum_{j=0}^{j_{max}} B_{ijk} \left(\Phi_c + \Phi_d\right) \tag{10}$$

where J_{ik} and E_{ik} is the spin and energy of the i-th excited state of the k-th nuclei, respectively. B_{ijk} is the matrix element for the $i \to j$ transition starting with k-th parent nuclei. G_k is temperature-dependent partition function for k-th nuclei (6). As in general both capture and decay is possible, for neutrinos we have:

$$\Phi_c + \Phi_d \equiv \Phi_c(\mathcal{E}_{\nu_e}, E_{ik} - E_{jk}, kT, +\mu_e) + \Phi_d(\mathcal{E}_{\nu_e}, E_{ik} - E_{jk}, kT, -\mu_e)$$

and for antineutrinos:

$$\Phi_c + \Phi_d \equiv \Phi_c(\mathcal{E}_{\bar{\nu}_e}, E_{ik} - E_{jk}, kT, -\mu_e) + \Phi_d(\mathcal{E}_{\bar{\nu}_e}, E_{ik} - E_{jk}, kT, +\mu_e).$$

Unit step function in (8) and (9) for $\mathcal{E}_\nu > 0$ automaticaly put zero into eq. (10) if decay/capture is not possible. Phase space factor depends on charge Z_k of the nuclei, but in actual spectrum reconstruction procedure (Sect. IV B) Coulomb corrections were neglected in Eqns. (8, 9).

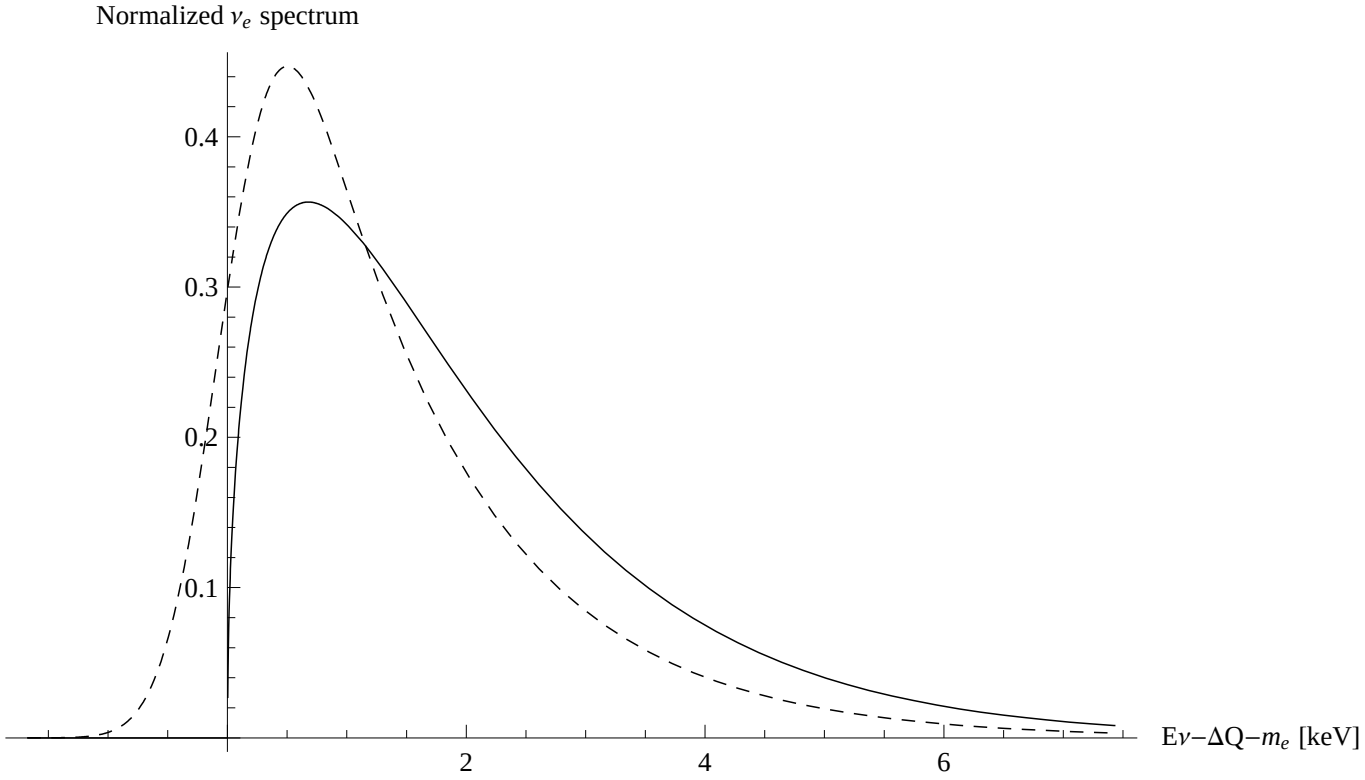

FIG. 6: Normalized neutrino spectrum for solar ^{7}Be electron capture neutrino line computed according to (8) (solid) and state-of-art result computed by Bahcall ([52], Eq. (46)) including thermal motions of nuclei (dashed).

As an introduction into the problem we start simplified analysis based on neutrino flux and average energy of the emitted neutrinos, i.e. data usually published in the context of applications in the astrophysics [34–36, 53–55]. Typical behavior of the ν_e and $\bar{\nu}_e$ emissivities as a function of Y_e is presented in Fig. 8. Temperature and density dependence of emissivity and average energy is presented in Fig. 10.

As Y_e decrease, ν_e flux (produced mainly in electron captures on protons and heavy nuclei) also tends to decrease. On the other hand, decrease in Y_e cause increase in $\bar{\nu}_e$ flux. Usually antineutrino emissivity peaks due to beta decays of the heavy nuclei and rise again due to positron capture on neutrons and neutron decay, cf. Fig. 8. For almost all pairs (kT, ρ) we can find Y_e value (Fig. 9) where ν_e flux is equal to $\bar{\nu}_e$ flux. These threshold values are particularly interesting for neutrino astronomy, as they might lead to strong neutrino and antineutrino emission without further neutronization, i.e. altering constraints from nucleosynthesis studies. Increasing $\bar{\nu}_e$ emission cause neutronization to stop a little bit earlier than derived from e.g. expansion of matter and related decrease in density alone in calculations concentrated on electron captures only. Neutronization stops because degeneracy is lifted or because Y_e becomes too low and positron captures/beta decays start to dominate. Surprisingly, these critical Y_e values (defined as Y_e for which $\dot{Y}_e = 0$, Fig. 8) vary in broad range (Fig. 9), reaching values close to $Y_e = 0.875$ i.e. primoidal BBN mixture of hydrogen and helium for low densities and $kT = 0.5 \ldots 0.8$. On the other hand, for highest densities ($\rho > 10^{11}$ g/cm^3) and temperatures kT$\simeq$0.8 MeV equilibrium sets at $Y_e = 0.2 \ldots 0.3$. It is important to notice, that due to low accuracy of the weak rates derived from FFN tables and variability of the NSE state with Y_e (Fig. 5), Figure 9 provides only a very approximate outlook of critical values. "Islands" in Fig. 9 might not be real, as well as really existing ones missing. Critical value[10] is also very important for NSE timescales, as ,,stalled" Y_e provide additional time without breaking assumption on quasistatic Y_e evolution.

Competition between ν_e and $\bar{\nu}_e$ emission (Fig. 9) is usually described in terms of the balance between electron captures (mainly on p, ^{56}Ni and ^{55}Co) and β^- decays of the heavy nuclei [38]. However, for Y_e outside range of 0.35..0.45 the most important process leading to the $\bar{\nu}_e$ is the positron capture on neutrons.

It is interesting to compare cooling efficiency of the NSE neutrino process and thermal processes. We have also

[10] State with $\dot{Y}_e = 0$ is frequently refereed to as *kinetic beta equilibrium.*

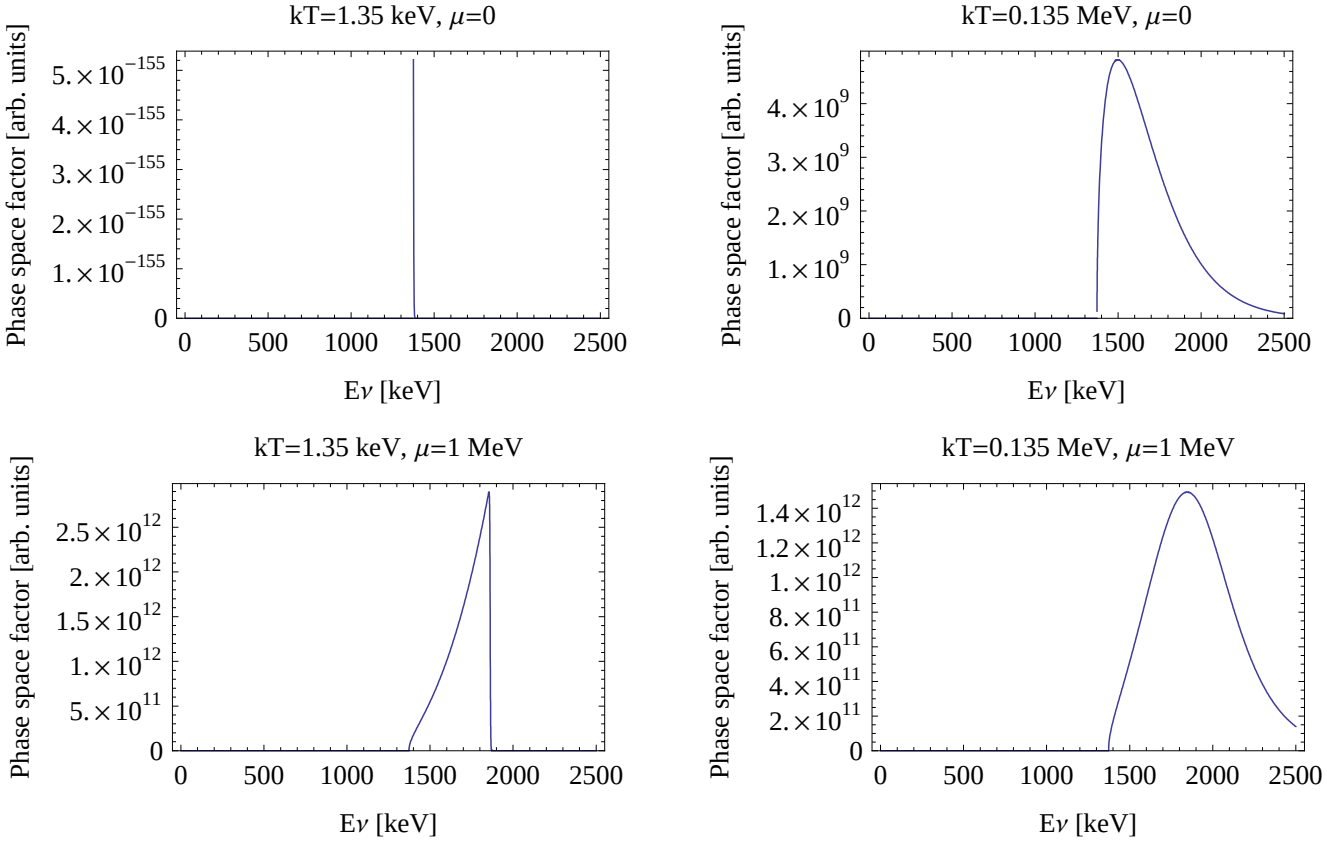

FIG. 7: Influence of the degeneracy (large μ) and high temperatures (large kT) on the electron capture neutrino spectrum, between fixed pair of energy levels in the parent and daughter nuclei, here ground states of ^{7}Be and ^{7}Li, respectively. Upper-left figure is for solar neutrinos (laboratory conditions), lower-left for cold degenerate electron gas, upper-right for high temperature and lower-right combines degeneracy and high temperature.

extracted emission due to free nucleons because (1) it dominates over wide range of densities and temperatures (2) rates and spectra are very reliable and well established in contrast to nuclei contribution. Results are sensitive to Y_e, but presented in Fig. 10 situation is typical for processes in evolutionary advanced astrophysical phenomena.

B. Computational procedure for NSE neutrino spectrum

As we want to obtain results in agreement with FFN tables, and due to lack of the related input data we follow procedure of [51] i.e. analytical representation of the spectrum. We use slightly modified approach. For given value of the temperature kT, μ and $\langle \mathcal{E}_\nu \rangle$ effective ΔQ is computed from (8) or (9). Spectrum obtained this way is then renormalized to FFN total rate. If capture rate dominates and $\langle \mathcal{E}_\nu \rangle > 3\,kT$ we use (8). Otherwise (for $\beta^\pm$ "contaminated" rate) (9) has been used for individual nuclei. Exact formula (8) for capture on free nucleons has been used. Spectra of the individual nuclei has been added and tabulated. Typical result of the procedure has been presented in figures 11-22.

Noteworthy, while original FFN tables include approximate information on spectrum in the form of capture/decay rate and average neutrino/antineutrino energy, tables prepared according to [37], e.g. Table 2 of [56] may be at first sight *explicite* used to form approximate neutrino energy spectrum as follows. Spectrum used by [51] is simplified form of eq. (8):

$$\Phi(\mathcal{E}_\nu, \Delta Q, kT, \mu_e) = \frac{\ln 2}{\langle ft \rangle {m_e}^5} \frac{\mathcal{E}_\nu^2 (\mathcal{E}_\nu - \Delta Q)^2}{1 + \exp\left[(\mathcal{E}_\nu - \Delta Q - \mu_e)/kT\right]} \Theta(\mathcal{E}_\nu - \Delta Q - m_e), \tag{11}$$

where all used quantities are tabulated by [56]. Unfortunately, this works only for weak rates dominated by the electron captures. For other rates normalization of the spectrum (11) is wrong. Additionally, effective $\lg \langle ft \rangle$ values

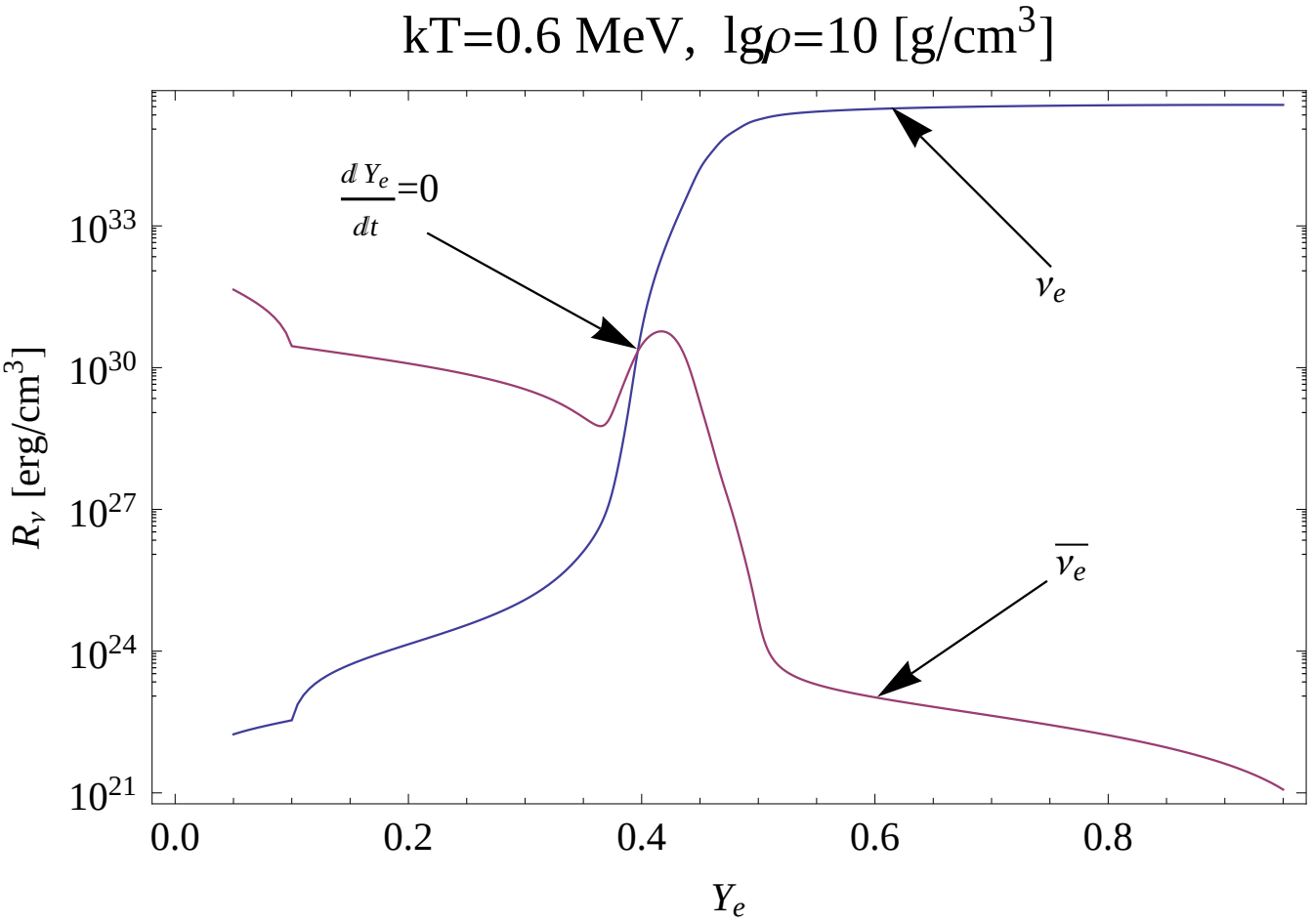

FIG. 8: Neutrino and antineutrino emissivities as a function of Y_e. Critical Y_e defined as $\dot{Y}_e = 0$ is visible as crossing point of neutrino and antineutrino particle emission rates.

also assume rate dominated by the captures. This is usually valid assumption for ν_e emission. But except for $e^+(n,p)\bar{\nu}_e$ dominated region, antineutrino emission is dominated by the β^- decays.

If capture dominates, formula (11) may serve as an upper limit estimate for high energy tail of the positron/electron capture spectrum. For $\mathcal{E}_\nu > 2Q$ we have:

$$\Phi(\mathcal{E}_\nu, \Delta Q, kT, \mu_e) < \mathcal{E}_\nu^4 e^{-\mathcal{E}_\nu/kT} e^{(Q-\mu)/kT}$$

and total flux above $> 2Q$ is:

$$8e^{-(Q+\mu)/kT} kT(3kT^4 + 6kT^3Q + 6kT^2Q^2 + 4kTQ^3 + 2Q^4)$$

Using formulae above, one can be show that average neutrino energy from electron (positron) capture is always $\langle \mathcal{E}_{\nu_e} \rangle > 3\,kT$. Therefore average energy below $3\,kT$ means significant fraction of the positron (electron) decay. Incidentally, $3\,kT$ is also mean energy for β^- decay as long as $m_e \ll Q < \mu$. Due to these limitations it is not possible to restore both capture and decay spectra from FFN-like data in unique way. Therefore, our approach is not satisfactory, but nothing more can be done using FFN-like tables, i.e. all available published results up to present. Unfortunately, spectrum reconstruction in the above form might lead to fake spectral features. If $\langle \mathcal{E}_\nu \rangle > 3\,kT$, for given average neutrino energy three distinct effective Q-values exist: pure capture, pure decay and mixed capture plus decay. If $\langle \mathcal{E}_\nu \rangle \leq 3\,kT$ two or one Q-values exist, depending on capture contribution. Fortunately, situation where captures and decays contribute at similar level is very rare in FFN tables. Nevertheless, accurate spectrum reconstruction is very difficult for these cases, which are of our interest, due to possible emission of high-energy neutrinos. We discuss this general problem in the last section.

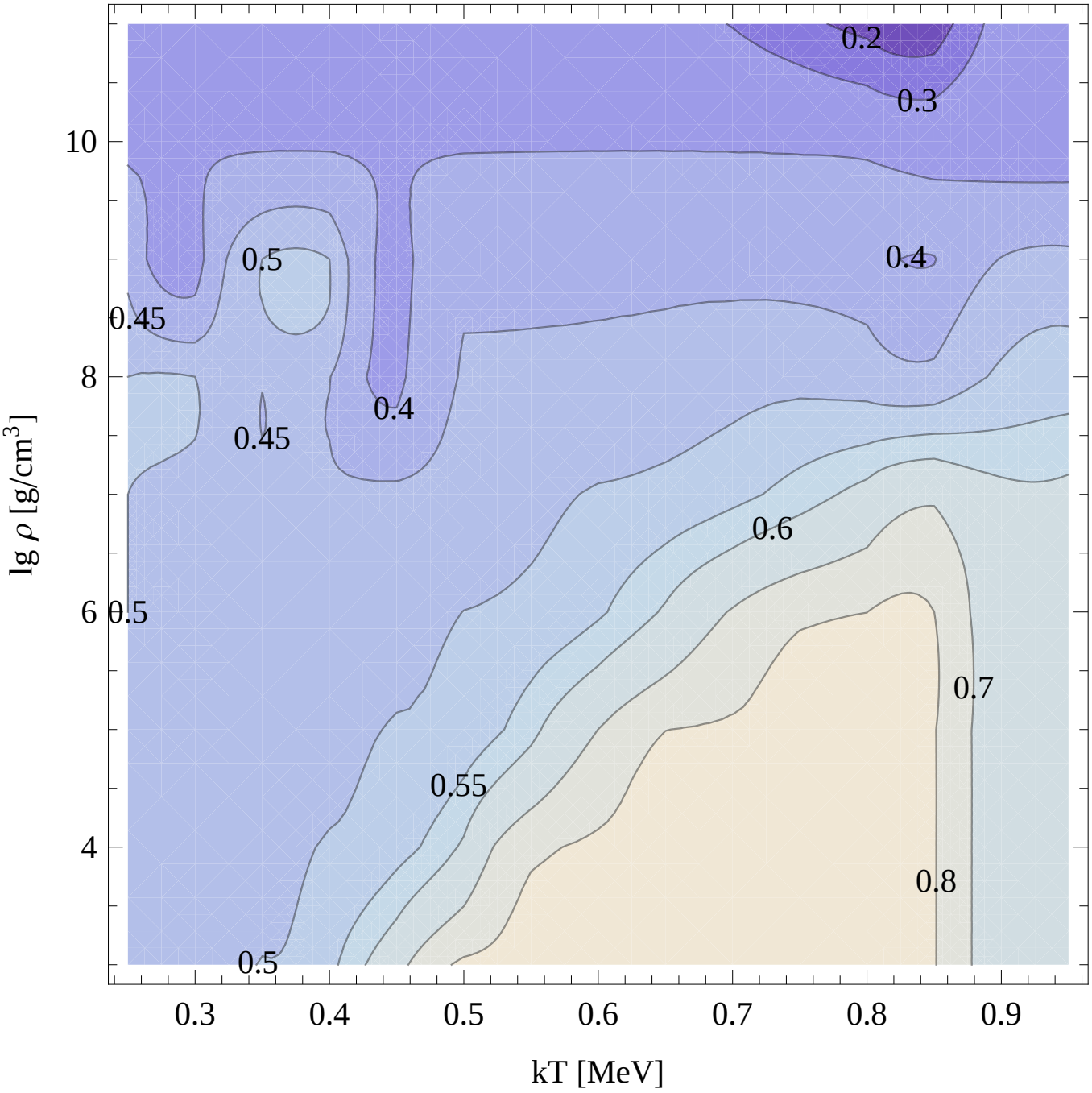

FIG. 9: Critical Y_e computed as explained in Fig. 8 for range of considered temperatures and densities.

C. Neutrino spectrum

In presentation of results we have included spectrum from thermal pair and plasma processes for comparison. In practice, thermal and weak processes operate simultaneously. Moreover, thermal spectrum often dominates emission. Spectrum produced by nucleons is computed exactly. For nuclei we have used reconstruction procedure described in previous section.

Typical ν_e energy spectra are presented in Figs. 11-16. Dotted lines shod thermal processes. Energy hierarchy is always $\mathcal{E}_\nu^{\rm plasmaL} < \mathcal{E}_\nu^{\rm plasmaT} < \mathcal{E}_\nu^{\rm pair}$ so no mistake is possible. Dot-dashed lines display electron capture on p, and dashed lines heavy nuclei contribution. Large diversity of spectra do not allow for simple description. For $Y_e = 0.1$ emission is dominated by captures on free protons and thermal processes. Note that *electron density* ρY_e (responsible

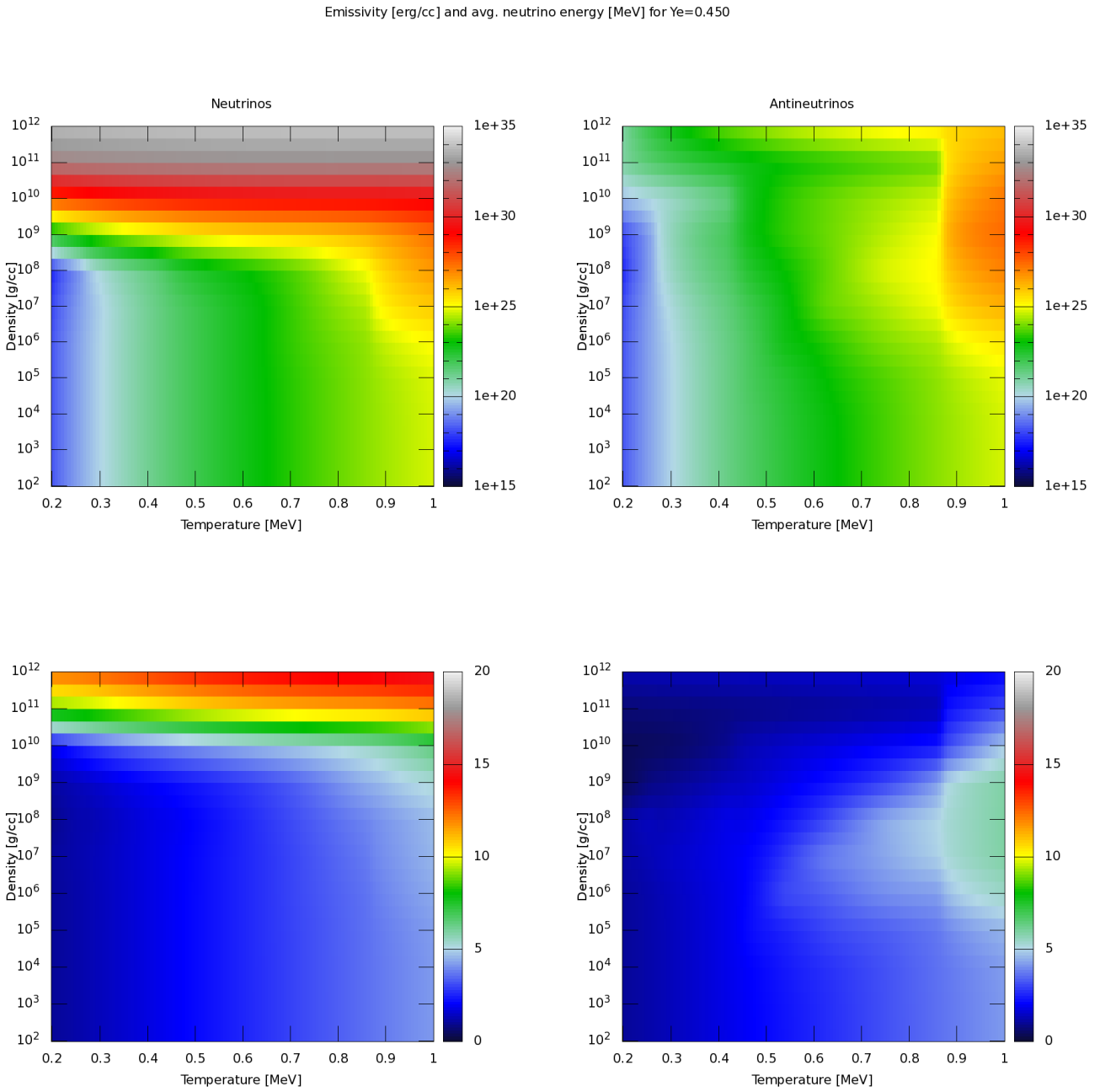

FIG. 10: Emissivity and $\langle \mathcal{E}_\nu \rangle$ for range of considered temperatures and densities. Situation for $Y_e = 0.45$ is typical, but see also animation for the whole considered range of $Y_e = 0.05 \ldots 0.95$ [42]. Dashed region is dominated by the thermal processes.

for electron chemical potential μ, i.e. affecting weak rates) is order of magnitude lower than actual density of matter in this case. For lowest presented temperature of 0.3 MeV ($T_9 \simeq 3.5$) and highest density $\rho = 10^{11}$ g/cm^3 spectrum is completely dominated by the plasmon decay, as expected. Rising temperature to 0.6 MeV ($T_9 \simeq 7$) do not change global view of the spectrum. For largest neutrino energies $\mathcal{E}_{\nu_e} > 6$ MeV, however, electron capture on protons dominate. Pair annihilation component also grows, but is still insignificant. For $kT = 0.9$ MeV ($T_9 \simeq 10.5$) low energy ($\mathcal{E}_{\nu_e} < 1$ MeV) part of the spectrum is still dominated by the plasma process, but both overall neutrino emissivity and high energy part is overwhelmingly dominated by electron capture on protons. This is combined result of large NSE fraction of free protons and weak rate. Other nuclei and pair process provide negligible contribution.

For $Y_e = 0.4$ and $\rho = 10^{11}$ g/cm^3 ν_e spectrum is overwhelmingly dominated by the captures on heavy nuclei.

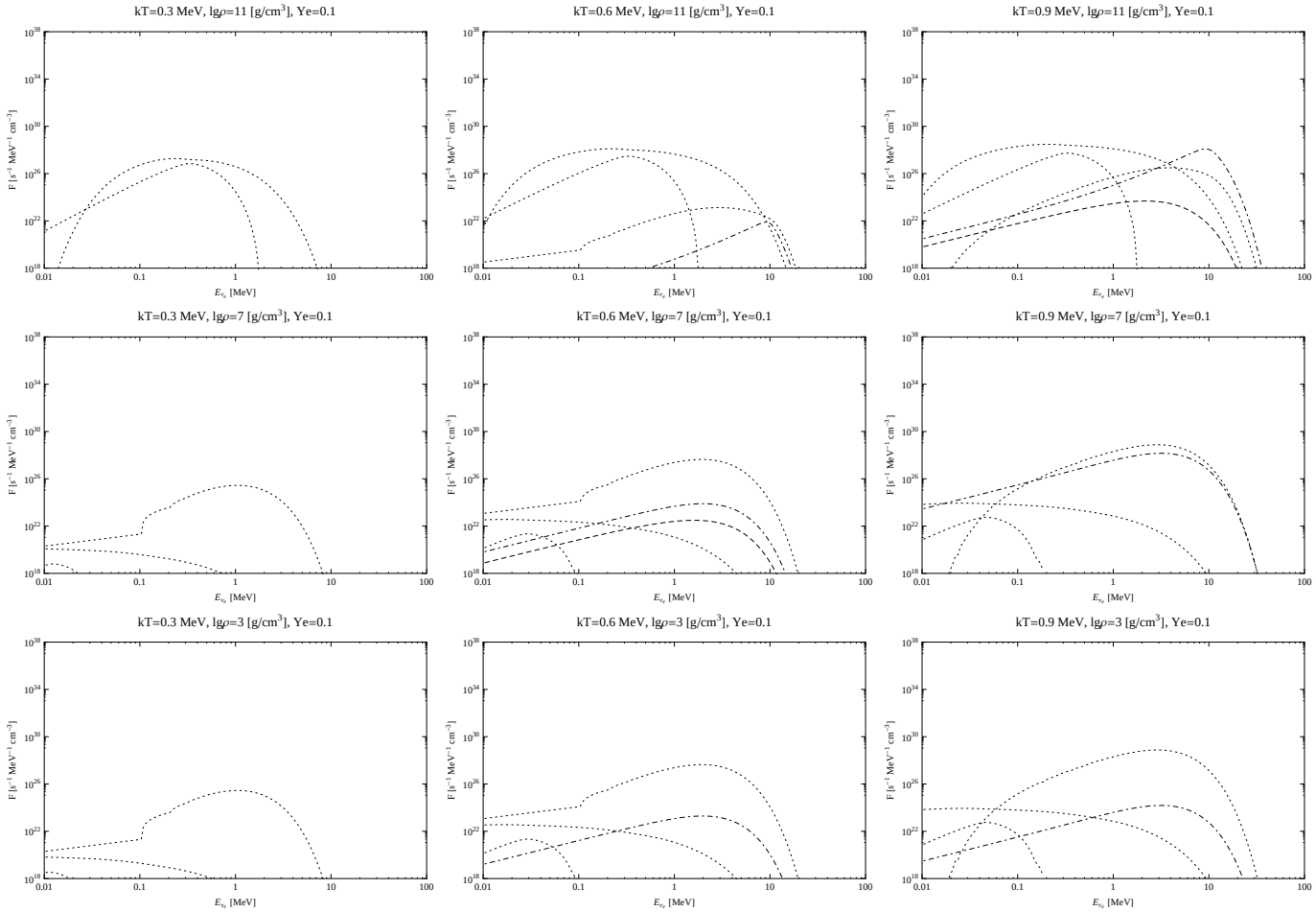

FIG. 11: Electron neutrino (ν_e) spectrum from the plasma under Nuclear Statistical Equilibrium (NSE) for $Y_e = 0.1$.

Plasmon decay adds only barely visible distortion of a spectrum below $\mathcal{E}_{\nu_e} < 1$ MeV for $kT = 0.3$ MeV. Remaining cases in Fig. 12 are dominated by the pair process. The only exception is visible on panel with $kT = 0.9$ MeV and $\rho = 10^7$ g/cm^3, where captures on free protons provide competing with pair annihilation contribution to the spectrum.

For $Y_e = 0.45$ situation is quantitatively very similar to $Y_e = 0.4$ case. However, flux due to heavy nuclei is now by a few orders of magnitude larger for highest density. Y_e increased further to 0.5 lead to even stronger ν_e flux. Additionally, spectrum for $kT = 0.3$ and $\rho = 10^7$ g/cm^3 becomes completely dominated by processes involving nuclei.

For $Y_e = 0.55$ contribution from protons becomes much more important due to increased abundance [29]. Contribution from thermal processes becomes far less important and limited to the lowest densities. Situation is even more pronounced for extreme case considered with $Y_e = 0.87$.

D. Antineutrino spectrum

Antineutrino spectrum, presented in Figs. 17-22, emitted under NSE is completely different than ν_e spectrum emitted with identical values of temperature, density and electron fraction. Line coding is similar to ν_e spectrum, but now dot-dashed line show neutron decay and positron capture on neutron. Total $\bar{\nu}_e$ flux never approach values as large as for ν_e. Therefore, kinetic beta equilibrium can be achieved only under conditions related to moderate neutrino emissivities. Spectrum for $Y_e = 0.1$ is again dominated by thermal processes (plasma for highest and pair for lowest densities) and processes involving free neutrons. As both β^- decay and ϵ^+ captures are possible for neutrons, spectrum has characteristic two-peak shape with a gap of $\Delta Q + 2\,m_e \simeq 2.3$ MeV width. Relative height of a peaks depends on blocking factors for e^-, growing with density, and amount of e^+ available for captures, growing with temperature. Similar pattern is expected for nuclei but due to reconstruction procedure multi peak spectra are approximated by a single peak function. Noteworthy, positron capture on neutrons produces $\bar{\nu_e}$ with relatively high energies, and tail

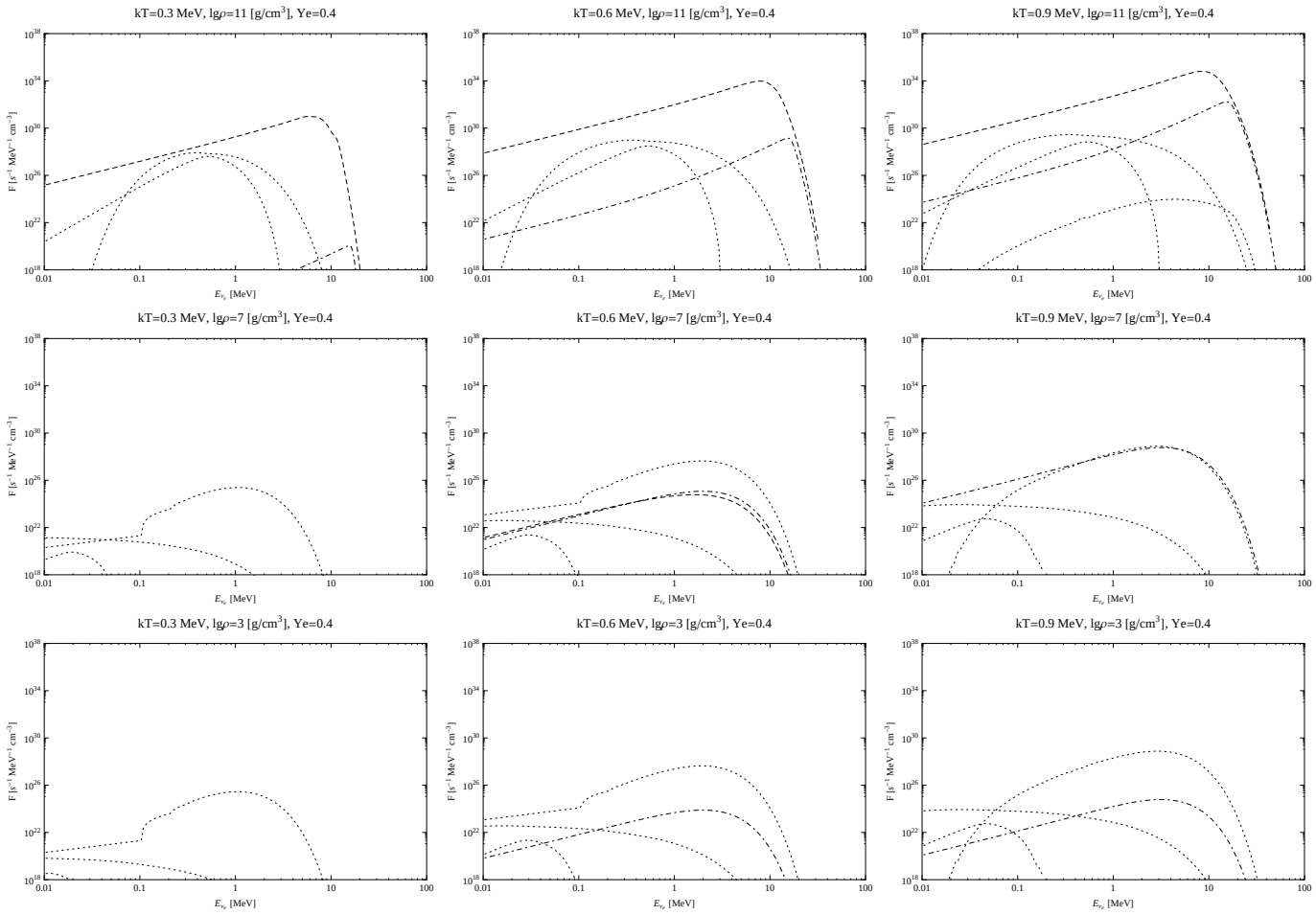

FIG. 12: Same as in Fig. 11 for $Y_e = 0.4$.

of a spectrum tends to be dominated by this process. For $Y_e = 0.1$ antineutrinos produced by positron capture on neutrons dominates high energy tail almost everywhere, except extreme cases: (1) lowest temperature highest density and (2) highest temperature lowest density.

For $Y_e = 0.4$ we are not surprised to see significant contribution from beta-decaying heavy nuclei. In contrast to ν_e emission, spectrum has a cutoff. This is visible in panel with $kT = 0.9$ MeV and $\rho = 10^{11}$ g/cm^3, where high energy tail is dominated by the pair annihilation process. For $\rho = 10^7$ g/cm^3 and $kT > 0.6$ MeV reaction $e^+ + n \to p + \bar{\nu}_e$ dominates due to high equilibrium fraction of both neutrons and positrons. For lower densities pair process dominates $\bar{\nu}_e$ emission. A bit surprisingly, situation quantitatively do not change for all values of $Y_e > 0.4$.

V. CONCLUSIONS

One of our important conclusions is related to typical way of publishing data on weak nuclear processes in astrophysics. This approach dates back into year 1980, and was introduced in famous paper [34]. Tables published by the FFN become standard in modern astrophysics. Upgrades [34, 55, 56] did not change structure of FFN tables. Unfortunately, FFN grid using mere 13x11 points is not enough to obtain precise results, as noted already by the FFN authors [37]. While we understand reasons to preserve this standard for 30 years, "reverse engineering" of FFN-like tables to get spectrum, as well as complicated interpolating procedure is impractical now. If one want to calculate spectrum precisely, without analytical approximate formula for individual nuclei, pre-calculated tables are useless. Much more convenient is the following set of data:

1. energy and spins for ground (i.e. mass of the nuclei) and excited states

2. weak transition matrix elements between all relevant pairs of the excited states for the parent and daughter

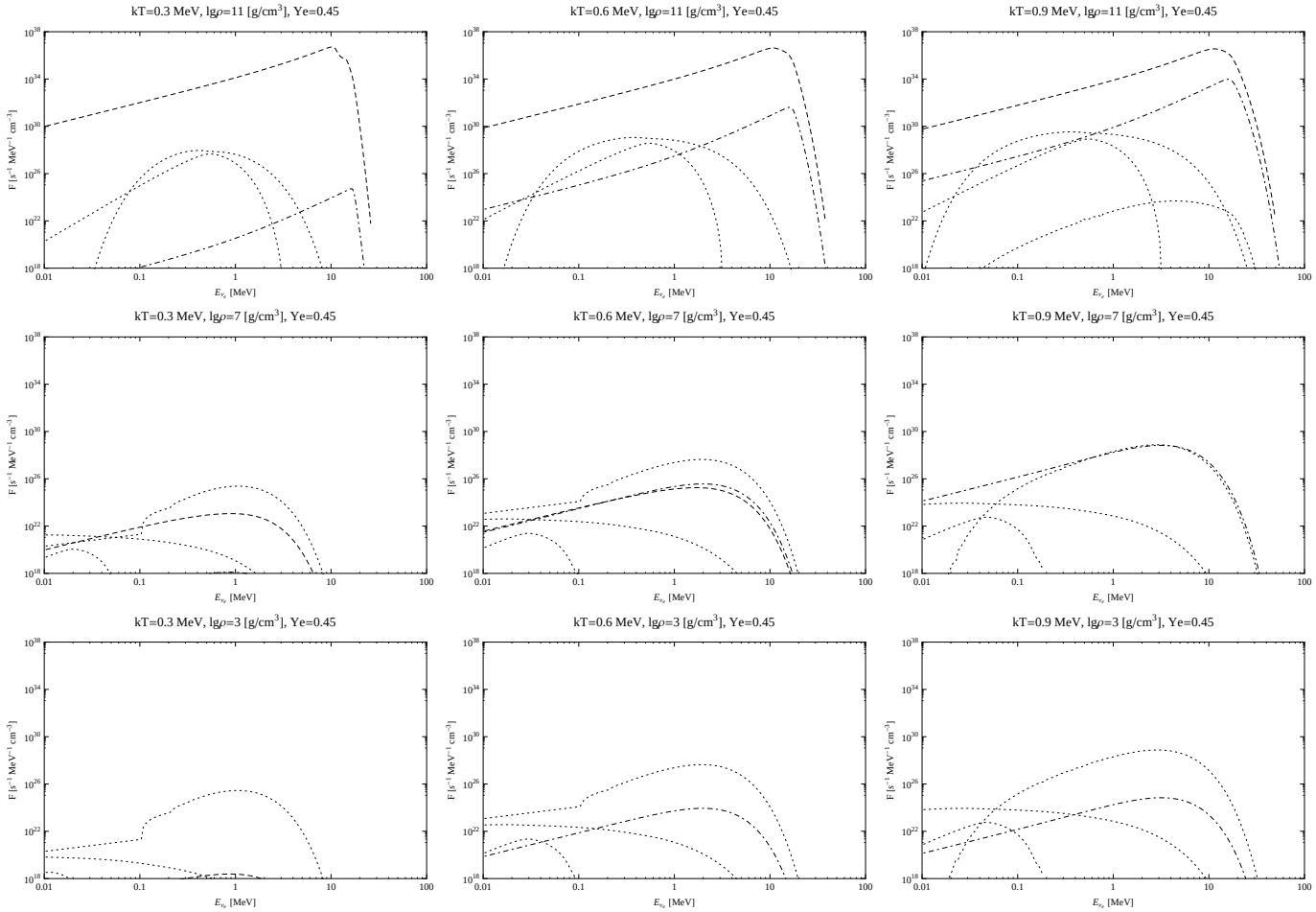

FIG. 13: Same as in Fig. 11 for $Y_e = 0.45$.

nuclei

Alternatively, tabulated spectrum for all $T - \rho Y_e$ pairs would be a good choice, with amount of stored data up to several megabytes. While such approach will increase amount of published numerical data by a factor of ~ 10, any ambiguity due to analytical representation of the spectra becomes non-existent. Information on contribution from individual nuclei is however lost this way.

Inspection of virtually any of the figures presented clearly show importance of both nuclear and thermal processes. Thermal emission, captures on free nucleons and nuclei should be included in consistent calculations. However, depending on subject, all combinations of these can be found in astrophysical applications. For example, type Ia supernova simulations include NSE emission but older simulations neglect neutrino emission at all or include electron captures only [19]. Other important regimes, core-collapse and pre-supernovae frequently neglect positron captures, particularly on neutrons. Estimates of the neutrino signal in detectors from pre-supernovae rely purely on thermal emission [57–59].

Ultimate goal which is beyond scope of the article is to know exactly (not approximately) neutrino spectrum from weak nuclear processes under NSE. In the past weak rates were usually integrated and only total neutrino flux (particle and energy) has been tabulated and presented to the public. We argue again, that this is not the best approach if one want to calculate neutrino spectrum. Without full input used to calculate rates we are unable to restore information lost in the integration. Typical (FFN-like) weak interaction tables are not sufficient. Tables of the excited states, spins and weak matrix elements for all considered nuclei will allow researchers to calculate both neutrino/antineutrino spectra and customized weak interaction rate tables.

Weak rates prepared in the FFN fashion (i.e. all published rates [34, 55, 56]), even those with tabulated effective $\lg \langle ft \rangle$, do not facilitate estimates of the neutrino spectrum. This is not surprise, as these rates were prepared for a different purposes: neutrino energy loss and neutronization. Maximal information on the spectrum extracted from FFN-like tables can be extracted as described in the paper. We re-tabulate effective $\lg \langle ft \rangle$ values and effective

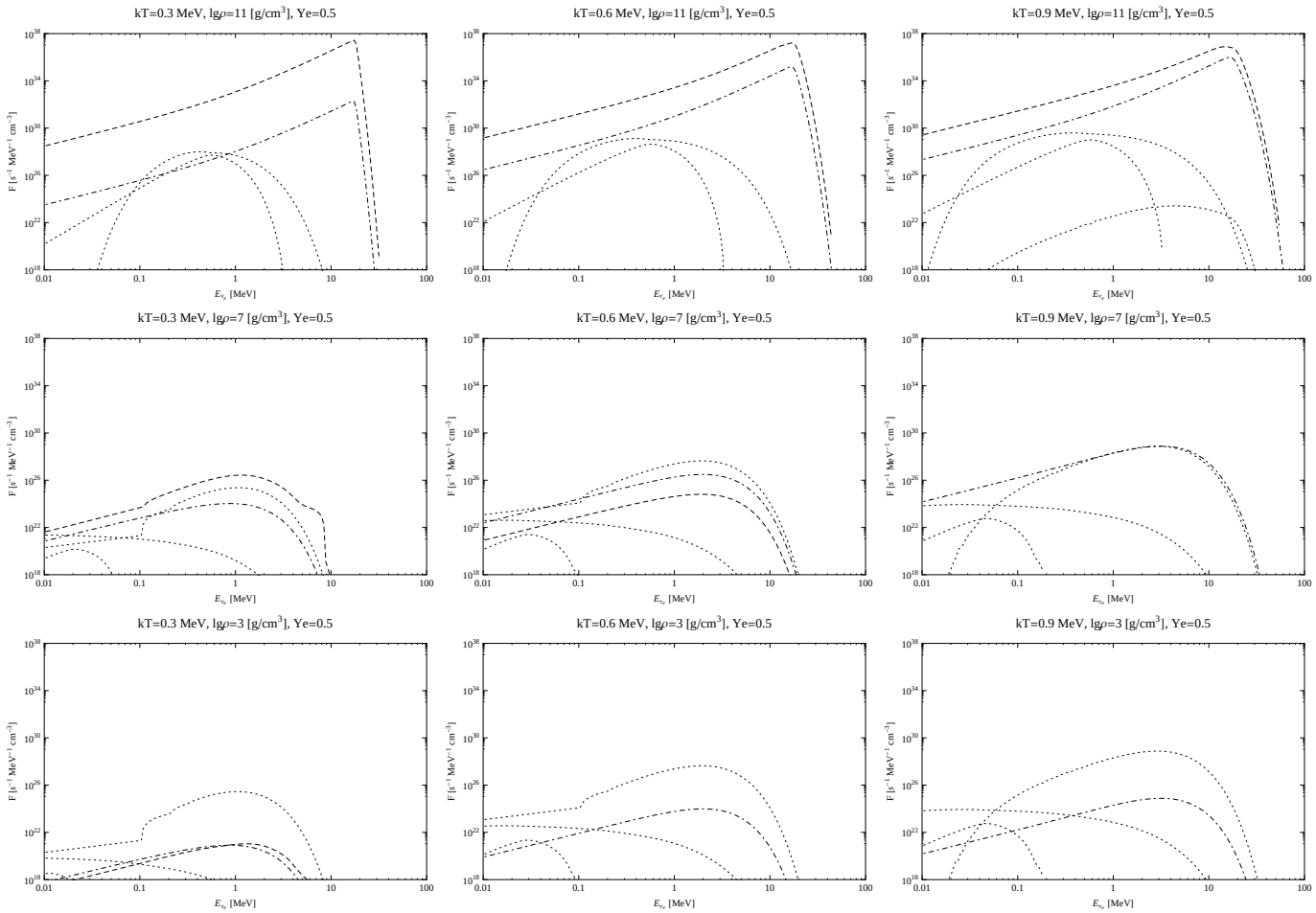

FIG. 14: Same as in Fig. 11 for $Y_e = 0.5$.

Q_{eff}-values for every grid point to get from (8) or (9) original total rate and average neutrino energy. If total rate is not dominated by the captures we switch from (8) to (9). This approach produce significant side effects if capture and decay rates are comparable. Neutron provides good example. Due to non-negligible contribution of $\bar{\nu}_e$'s from neutron decay, average energy differ from pure positron capture. Therefore effective spectrum has variable effective Q-value. Realistic positron (and electron as well) capture spectrum always start with energy equal to lowest Q-value. To sum up, the obvious next step in research is to give up pre-calculated tables of weak rates and re-calculate neutrino spectrum from scratch, using nuclear data and weak matrix elements as an input.

Despite difficulties, we managed to deliver some new results, as well as convenient computational methods and insights, on the NSE itself and related neutrino emission:

1. interpolating procedures for NSE abundances with number of convenient features: ability to pick out of NSE selected nuclei, computational time scaling linearly with number of nuclides and independent of the position in $T - \rho - Y_e$ space for full $Y_e = 0.05 \ldots 0.95$ range

2. fluxes, mean energies and approximate energy spectrum of the emitted neutrinos and antineutrinos separately for ν_e and $\bar{\nu_e}$

Our analysis was meant to be general, but we can identify some possible astrophysical targets for presented methods. NSE neutrino spectrum would be a good approximation for massive stars after Si burning and thermonuclear supernovae. Related research is underway. Developed procedures will be also useful also for analysis of neutrino signals from X-ray flashes, neutron stars, merger events, accretion disks and some types of cosmic explosions, e.g. pair-instability supernovae.

Electron antineutrino emission due to positron capture on neutrons provides strong and relatively high-energy flux for surprisingly large volume in $kT - \rho - Y_e$ space, cf. Fig. 10. Related thermodynamic conditions: $kT > 0.6$ and $\rho > 10^7$ g/cm^3 are not extremely exotic in cosmos, while antineutrino energy $\mathcal{E}_{\bar{\nu_e}} > 1.8$ MeV is prospective for

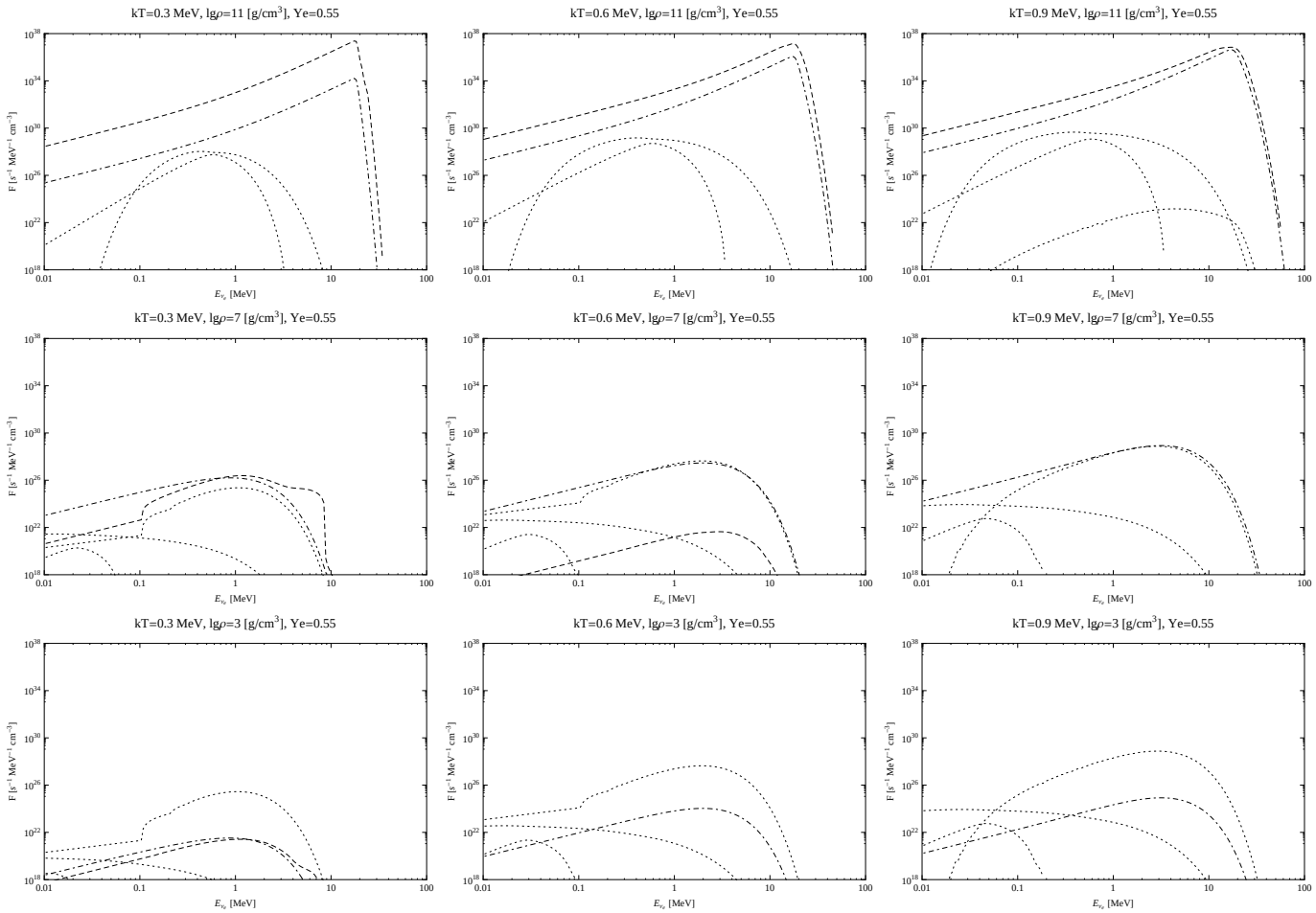

FIG. 15: Same as in Fig. 11 for $Y_e = 0.55$.

megaton-scale neutrino detectors [60]. Detection of strong ν_e flux above 5 MeV produced mainly due to captures on protons and heavy nuclei (cf. e.g. Fig. 14) is standard task for water Cherenkov [61–63] or liquid scintillator [64] using elastic scattering of electrons and protons as well [61, 65]. Therefore further investigation of NSE neutrinos, particularly in the unexplored region of large $0.87 > Y_e \gg 0.55$ should give researchers some additional hints for existence (or non-existence) of detectable astrophysical antineutrino sources.

Acknowledgments

We would like to thank Iwo Seitenzahl for discussion of the NSE calculations, and Tomasz Plewa for motivation and support of this work.

[1] D. Arnett, *Supernovae and nucleosynthesis* (Princeton University Press, 1996).
[2] G. S. Bisnovatyi-Kogan, *Stellar physics. Vol.1: Fundamental concepts and stellar equilibrium* (Springer, 2001).
[3] R. Kippenhahn and A. Weigert, *Stellar Structure and Evolution* (Springer-Verlag Berlin Heidelberg New York. Astronomy and Astrophysics Library, 1994).
[4] S. E. Woosley, A. Heger, and T. A. Weaver, Reviews of Modern Physics **74**, 1015 (2002).
[5] P. Young, D. Arnett, C. Meakin, and C. Fryer, Astrophysical Journal **629**, 69 (2005).
[6] M. Haft, G. Raffelt, and A. Weiss, Astrophys J. **425**, 222 (1994), astro-ph/9309014.
[7] E. M. Kantor and M. E. Gusakov, MNRAS **381**, 1702 (2007), arXiv:0708.2093.

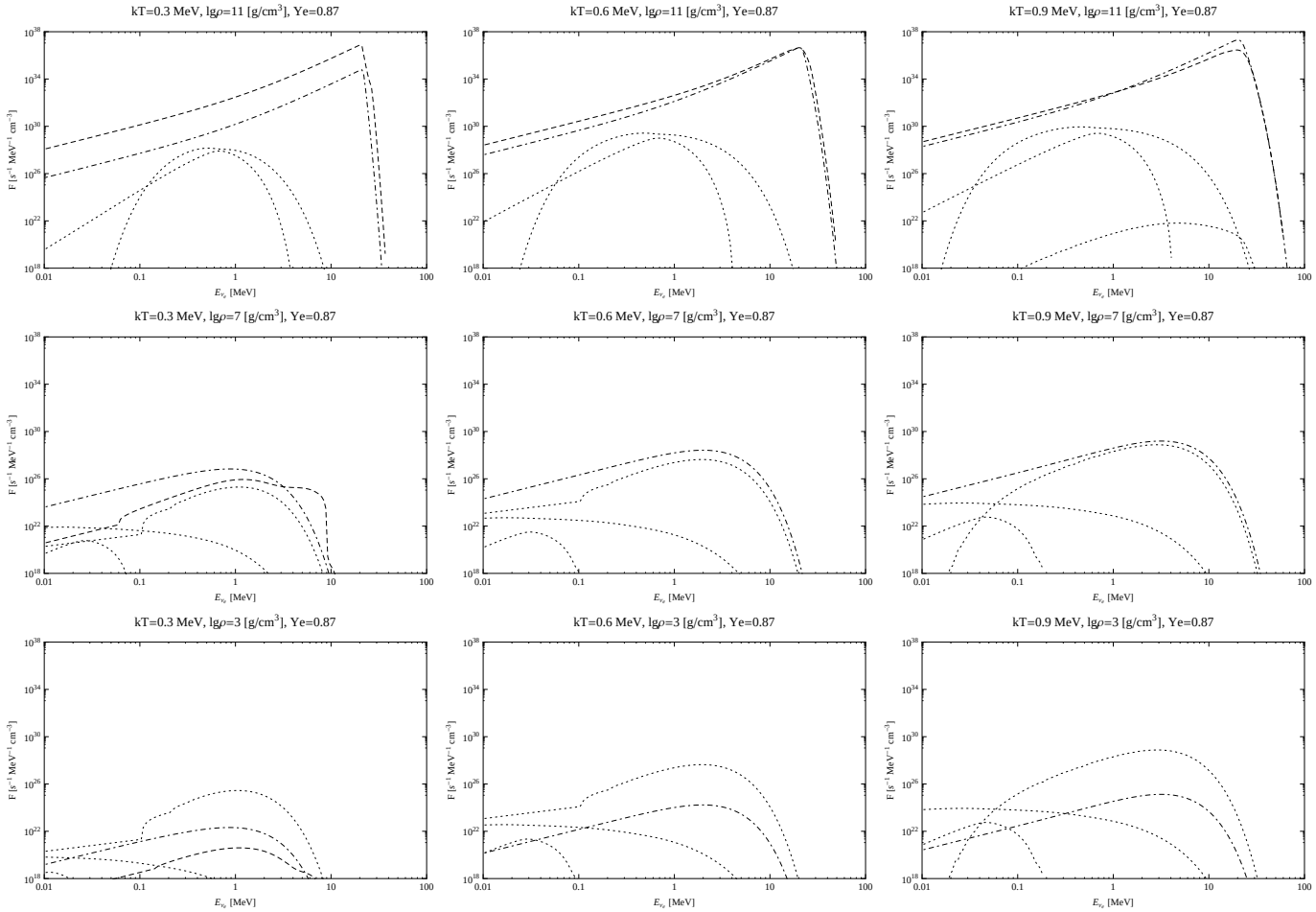

FIG. 16: Same as in Fig. 11 for $Y_e = 0.87$.

[8] S. W. Bruenn, C. J. Dirk, A. Mezzacappa, J. C. Hayes, J. M. Blondin, W. R. Hix, and O. E. B. Messer, Journal of Physics Conference Series **46**, 393 (2006), 0709.0537.

[9] R. Buras, H.-T. Janka, M. Rampp, and K. Kifonidis, A&A **457**, 281 (2006), arXiv:astro-ph/0512189.

[10] R. Buras, M. Rampp, H.-T. Janka, and K. Kifonidis, A&A **447**, 1049 (2006), arXiv:astro-ph/0507135.

[11] H. Duan, G. M. Fuller, J. Carlson, and Y.-Z. Qian, Physical Review Letters **100**, 021101 (2008), 0710.1271.

[12] J. W. Murphy and A. Burrows, ApJ **688**, 1159 (2008), 0805.3345.

[13] K. Nakazato, K. Sumiyoshi, and S. Yamada, ApJ **666**, 1140 (2007), 0705.4350.

[14] D. G. Yakovlev, A. D. Kaminker, O. Y. Gnedin, and P. Haensel, Physics Reports **354**, 1 (2001).

[15] L. Dessart, C. Ott, A. Burrows, S. Rosswog, and E. Livne, ArXiv e-prints **806** (2008), 0806.4380.

[16] S. Rosswog, R. Speith, and G. A. Wynn, MNRAS **351**, 1121 (2004), arXiv:astro-ph/0403500.

[17] D. Giannios, ArXiv e-prints **704** (2007), 0704.1659.

[18] D. Lazzati, R. Perna, and M. C. Begelman, MNRAS **388**, L15 (2008), arXiv:0805.0138.

[19] T. Kunugise and K. Iwamoto, Publications of the Astronomical Society of Japan **59**, L57+ (2007).

[20] S. E. Woosley, A. Heger, A. Cumming, R. D. Hoffman, J. Pruet, T. Rauscher, J. L. Fisker, H. Schatz, B. A. Brown, and M. Wiescher, ApJS **151**, 75 (2004), arXiv:astro-ph/0307425.

[21] I. R. Seitenzahl, D. M. Townsley, F. Peng, and J. Truran, Atomic Data and Nuclear Data Tables (2008).

[22] S. W. Bruenn, apjs **58**, 771 (1985).

[23] A. Burrows and T. A. Thompson, ArXiv Astrophysics e-prints (2002), astro-ph/0211404.

[24] C. Fröhlich, G. Martínez-Pinedo, M. Liebendörfer, F.-K. Thielemann, E. Bravo, W. R. Hix, K. Langanke, and N. T. Zinner, Physical Review Letters **96**, 142502 (2006), arXiv:astro-ph/0511376.

[25] A. Heger, E. Kolbe, W. C. Haxton, K. Langanke, G. Martínez-Pinedo, and S. E. Woosley, Physics Letters B **606**, 258 (2005), arXiv:astro-ph/0307546.

[26] J. Pruet, R. D. Hoffman, S. E. Woosley, H.-T. Janka, and R. Buras, ApJ **644**, 1028 (2006), arXiv:astro-ph/0511194.

[27] M. Misiaszek, A. Odrzywolek, and M. Kutschera, Physical Review D **74**, 043006 (pages 9) (2006), URL `http://link.aps.org/abstract/PRD/v74/e043006`.

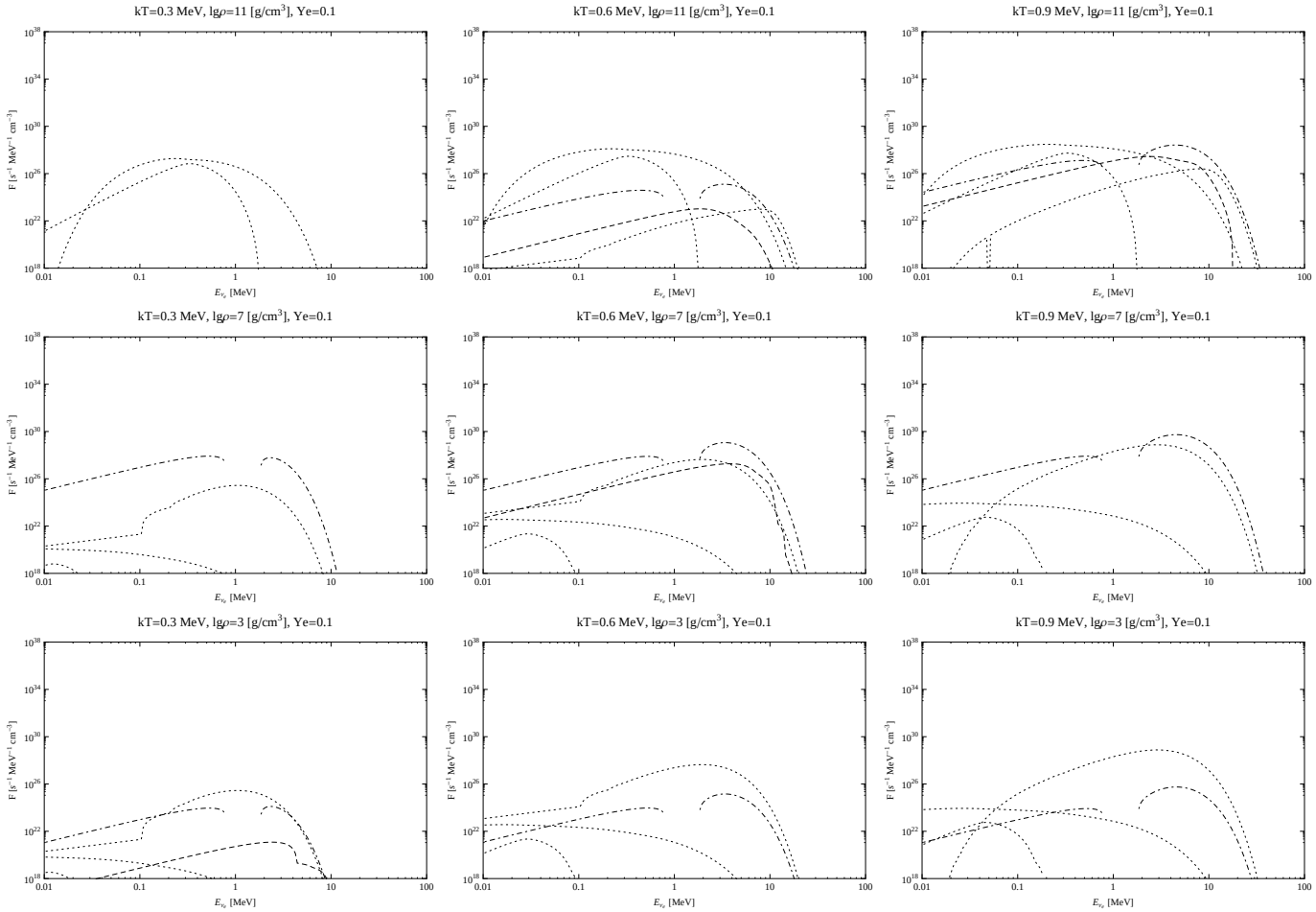

FIG. 17: Electron anti-neutrino ($\bar{\nu}_e$) spectrum from the plasma under Nuclear Statistical Equilibrium (NSE) for $Y_e = 0.1$.

[28] A. Odrzywolek, ArXiv e-prints **704** (2007), 0704.1222.
[29] I. R. Seitenzahl, F. X. Timmes, A. Marin-Laflèche, E. Brown, G. Magkotsios, and J. Truran, ArXiv e-prints **808** (2008), 0808.2033.
[30] F. E. Clifford and R. J. Tayler, MmRAS **69**, 21 (1965).
[31] V. S. Imshennik, S. S. Filippov, and A. M. Khokhlov, Pis ma Astronomicheskii Zhurnal **7**, 219 (1981).
[32] V. S. Imshennik, S. S. Filippov, and A. M. Khokhlov, Soviet Astronomy Letters **7**, 121 (1981).
[33] A. M. Khokhlov, A&A **245**, 114 (1991).
[34] G. M. Fuller, W. A. Fowler, and M. J. Newman, Astrophysical Journal Supplement Series **42**, 447 (1980).
[35] G. M. Fuller, W. A. Fowler, and M. J. Newman, ApJ **252**, 715 (1982).
[36] G. M. Fuller, W. A. Fowler, and M. J. Newman, ApJS **48**, 279 (1982).
[37] G. M. Fuller, W. A. Fowler, and M. J. Newman, ApJ **293**, 1 (1985).
[38] M. B. Aufderheide, I. Fushiki, S. E. Woosley, and D. H. Hartmann, ApJS **91**, 389 (1994).
[39] F. Timmes, *Cococubed.com*, http://cococubed.asu.edu/code_pages/nse.shtml (2008), URL `http://cococubed.asu.edu/code_pages/nse.shtml`.
[40] P. Mach, private communication (2008).
[41] B. Meyer, *Webnucleo: NSE CALCULATOR*, http://www.webnucleo.org/pages/nse/0.1/ (2008), URL `http://www.webnucleo.org/pages/nse/0.1/`.
[42] A. Odrzywolek, *PSNS code*, http://th-www.if.uj.edu.pl/psns/ (2005-2007), URL `http://th-www.if.uj.edu.pl/psns/`.
[43] W. R. Inc., *MATHEMATICA 7.0 IsotopeData[]*, http://reference.wolfram.com/mathematica/note/IsotopeDataSourceInformation.h (2008), URL `http://reference.wolfram.com/mathematica/note/IsotopeDataSourceInformation.html`.
[44] J. Golak, private communication (2008).
[45] L. E. Williams, C. J. Batty, B. E. Bonner, C. Tschalär, H. C. Benöhr, and A. S. Clough, Physical Review Letters **23**, 1181 (1969).
[46] D. R. Tilley, H. R. Weller, and H. H. Hasan, Nuclear Physics A **474**, 1 (1987).
[47] J. N. Bahcall, Phys. Rev. **126**, 1143 (1962).

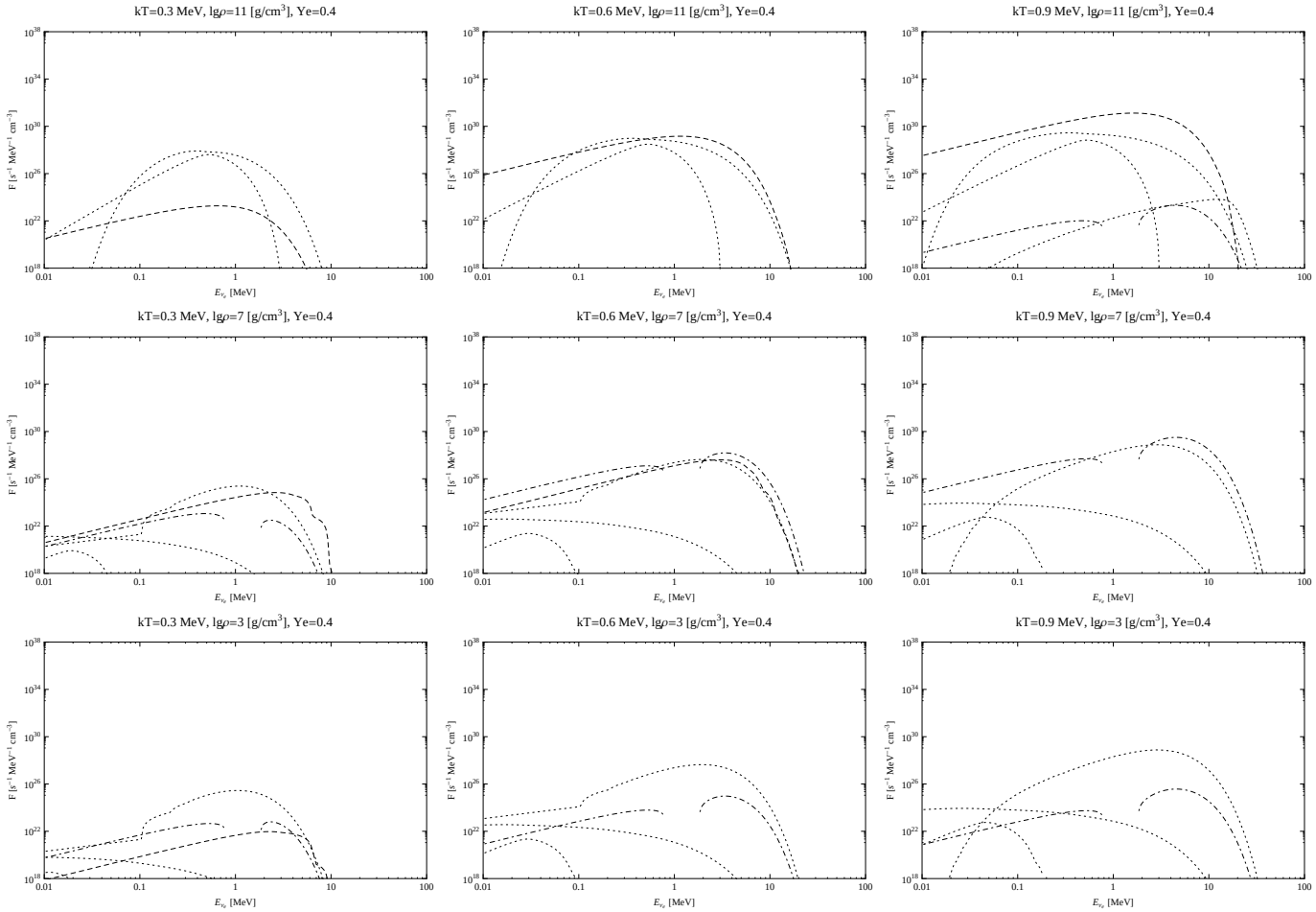

FIG. 18: Same as in Fig. 17 for $Y_e = 0.4$.

[48] J. N. Bahcall, Phys. Rev. **128**, 1297 (1962).
[49] J. N. Bahcall, *Neutrino astrophysics* (Cambridge and New York, Cambridge University Press, 1989, 584 p., 1989).
[50] S. Enomoto, PhD Thesis, Tohoku University (2005).
[51] K. Langanke, G. Martínez-Pinedo, and J. M. Sampaio, Phys. Rev. C **64**, 055801 (2001), arXiv:nucl-th/0101039.
[52] J. N. Bahcall, Phys. Rev. D **49**, 3923 (1994), arXiv:astro-ph/9401024.
[53] E. Caurier, K. Langanke, G. Martínez-Pinedo, and F. Nowacki, Nuclear Physics A **653**, 439 (1999), arXiv:nucl-th/9903042.
[54] K. Langanke and G. Martinez-Pinedo, Nuclear Physics A **673**, 481 (2000), arXiv:nucl-th/0001018.
[55] J.-U. Nabi and K. H. V., Atomic Data and Nuclear Data Tables **88**, 237 (2004).
[56] K. Langanke and G. Martínez-Pinedo, Atomic Data and Nuclear Data Tables **79**, 1 (2001).
[57] A. Odrzywolek, in *Twenty Years after SN1987A* (2007), URL `http://sn1987a-20th.physics.uci.edu/`.
[58] A. Odrzywolek, M. Misiaszek, and M. Kutschera, Astroparticle Physics **21**, 303 (2004).
[59] A. Odrzywolek, M. Misiaszek, and M. Kutschera, Acta Phys. Pol. B **35**, 1981 (2004).
[60] M. D. Kistler, H. Yuksel, S. Ando, J. F. Beacom, and Y. Suzuki, ArXiv e-prints (2008), 0810.1959.
[61] M. Fechner and C. Walter (2009), http://arxiv.org/abs/0901.1950v1.
[62] T. Abe, H. Aihara, C. Andreopoulos, A. Ankowski, A. Badertscher, G. Battistoni, A. Blondel, J. Bouchez, A. Bross, A. Bueno, et al., *Detectors and flux instrumentation for future neutrino facilities* (2007), URL `http://www.citebase.org/abstract?id=oai:arXiv.org:0712.4129`.
[63] A. de Bellefon, J. Bouchez, J. Busto, J. E. Campagne, C. Cavata, J. Dolbeau, J. Dumarchez, P. Gorodetzky, S. Katsanevas, M. Mezzetto, et al., *Memphys:a large scale water cerenkov detector at fr 'ejus* (2006), URL `http://www.citebase.org/abstract?id=oai:arXiv.org:hep-ex/0607026`.
[64] S. Katsanevas, Acta Physica Polonica B **37**, 2115 (2006).
[65] J. F. Beacom, W. M. Farr, and P. Vogel, Phys. Rev. D **66**, 033001 (2002), arXiv:hep-ph/0205220.

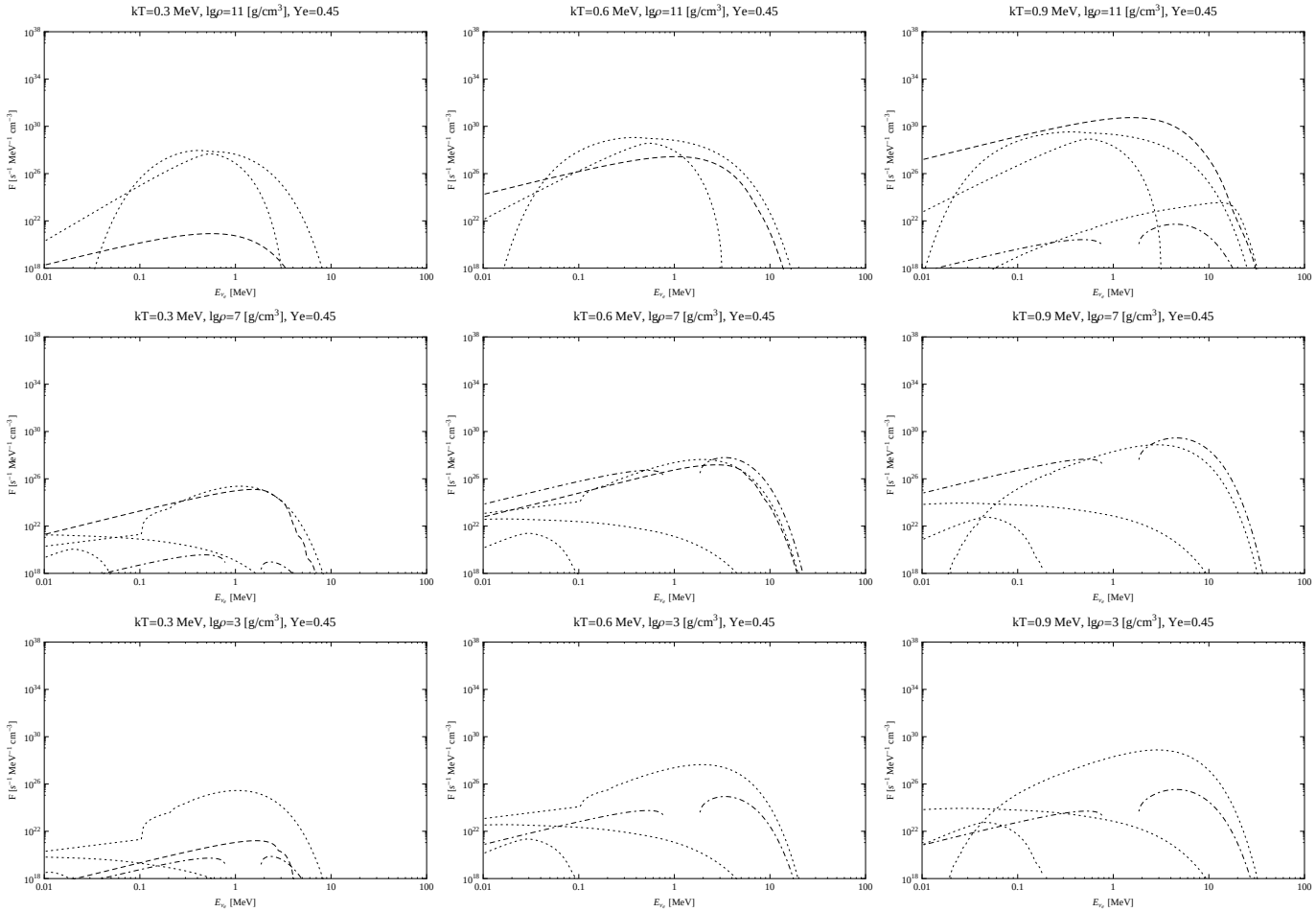

FIG. 19: Same as in Fig. 17 for $Y_e = 0.45$.

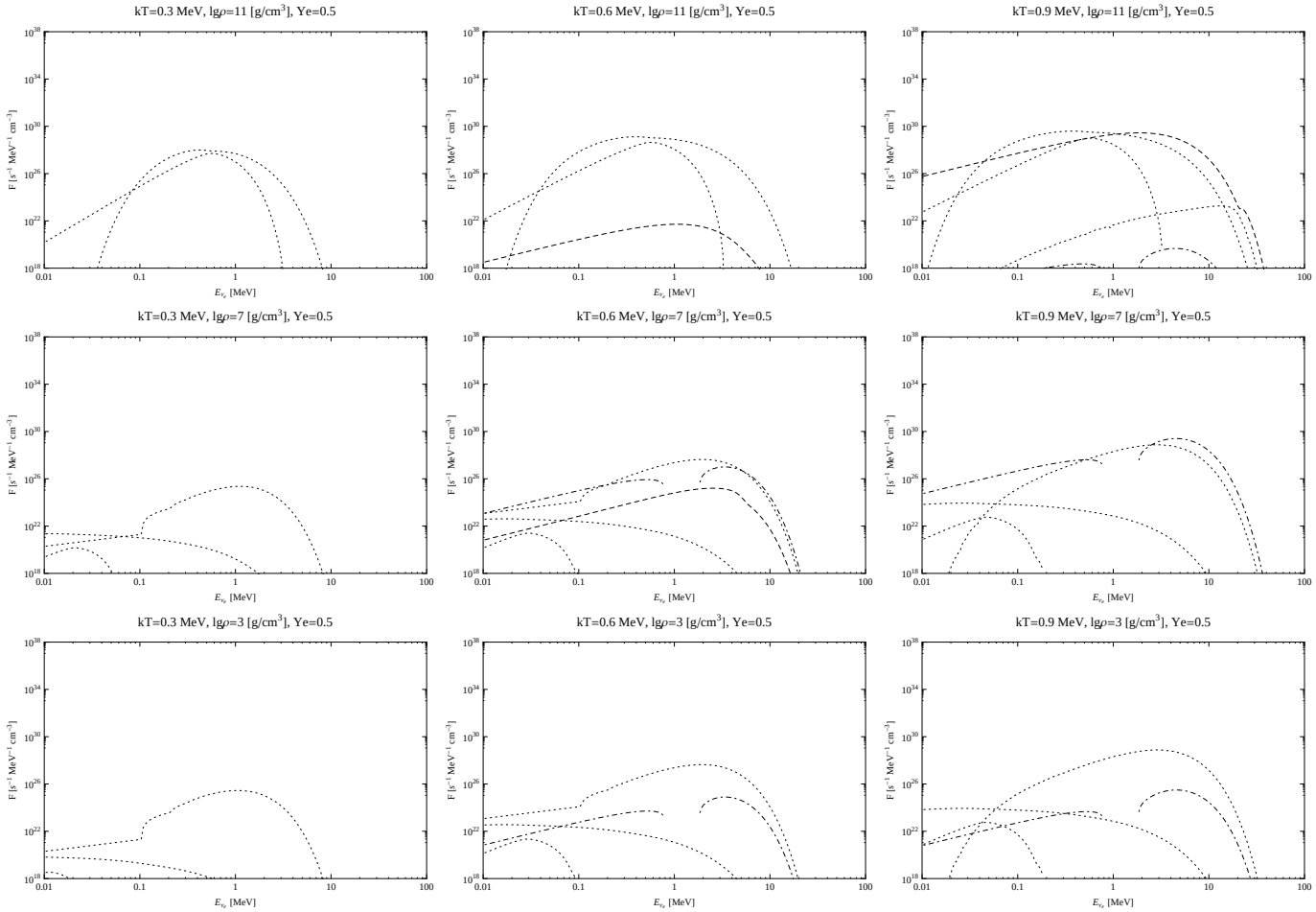

FIG. 20: Same as in Fig. 17 for $Y_e = 0.5$.

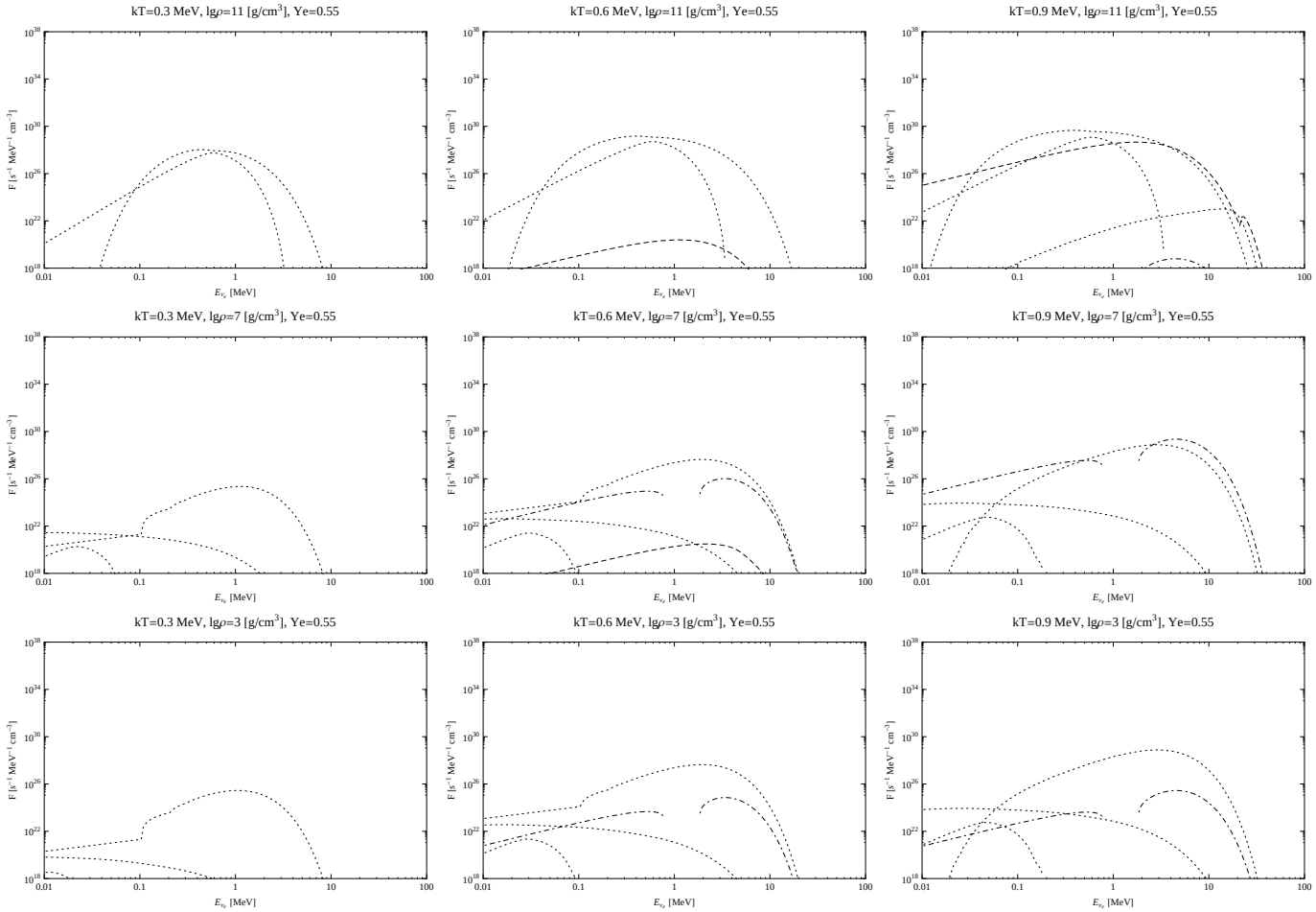

FIG. 21: Same as in Fig. 17 for $Y_e = 0.55$.

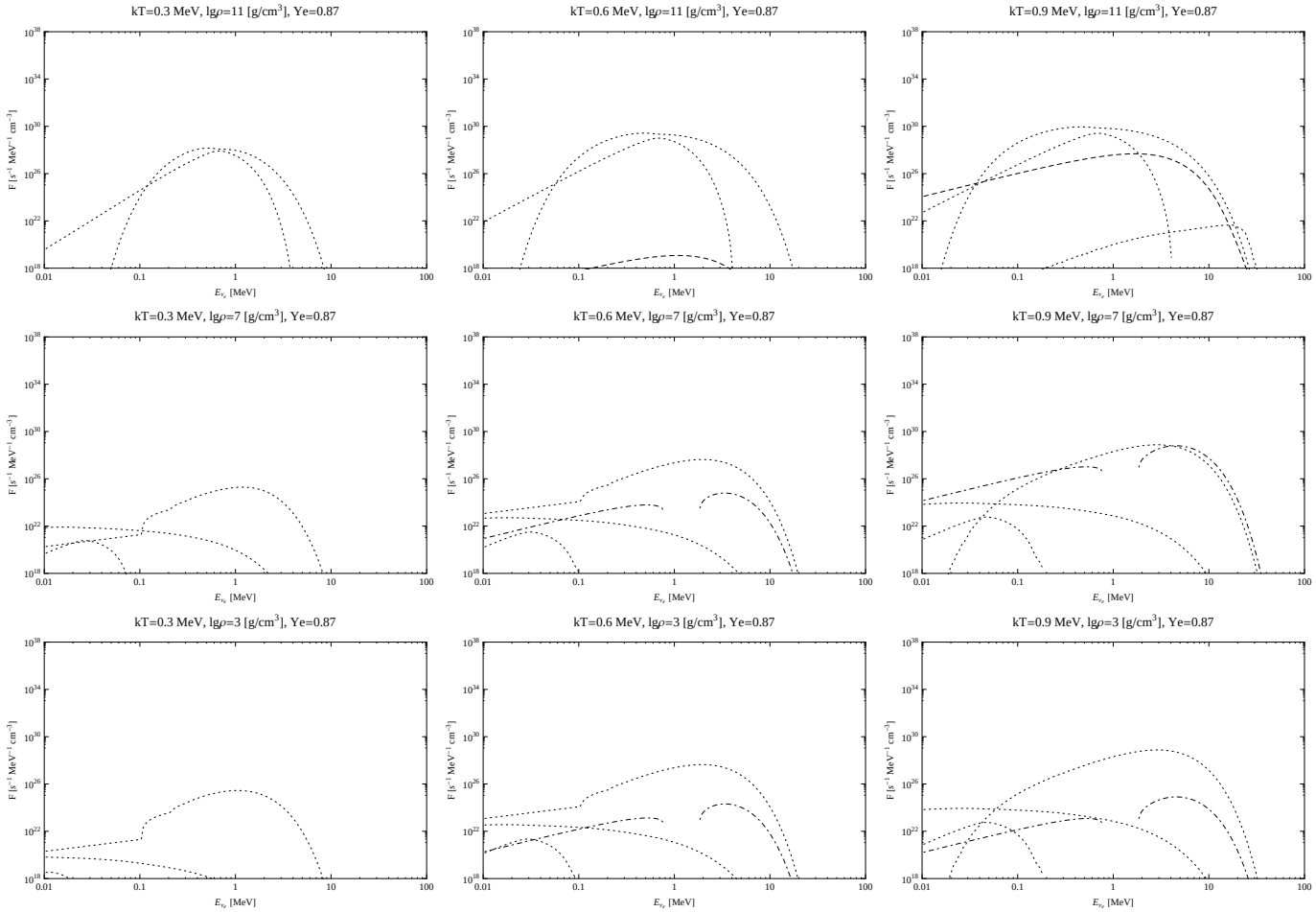

FIG. 22: Same as in Fig. 17 for $Y_e = 0.87$.